

Scale law of sCO₂ coal fired power plants regarding system performance dependent on power capacities

Chao Liu^a, Jinliang Xu^{a,b,*}, Mingjia Li^c, Zhaofu Wang^a, Zeyu Xu^a, Jian Xie^{a,b}

^a Beijing Key Laboratory of Multiphase Flow and Heat Transfer for Low Grade Energy Utilization, North China Electric Power University, Beijing 102206, China

^b Key Laboratory of Power Station Energy Transfer Conversion and System (North China Electric Power University), Ministry of Education, Beijing 102206, China

^c Key Laboratory of Thermo-Fluid Science and Engineering of Ministry of Education, School of Energy & Power Engineering, Xi'an Jiaotong University, Xi'an, Shaanxi 710049, China

ARTICLE INFO

Keywords:

sCO₂ cycle
Scale law
Pressure drop
Partial flow mode
Thermal efficiency

ABSTRACT

Once supercritical carbon dioxide (sCO₂) cycle is used for coal fired power plant with conventional boiler design (total flow mode TFM), ultra-large pressure drop of sCO₂ boiler occurs to suppress system efficiency, thus we proposed partial flow mode (PFM). A CO₂ stream is segmented into two parallel lines, each having half flow rate and half length. The effectiveness of PFM was examined at various power capacities (net power output W_{net}) covering 50–1000 MWe. A numerical model is established by coupling thermodynamic cycle of system and thermal-hydraulic characteristics of boiler. Scale laws of boiler size, mass flux and pressure drop in boiler tubes are developed, agreeing with numerical simulation results. We show that with increase of W_{net} , TFM increases pressure drops to generate additional pressure and load for compressors. This effect not only increases energy loads, but also raises exergy destructions for all components, deteriorating the first and second law efficiencies of the system. Compared with TFM, PFM reduces pressure drops according to the 1/8 criterion, the pressure drop penalty effect is eliminated to have much higher efficiencies than TFM. Because at smaller W_{net} such as 100 MWe, sCO₂ boiler has larger surface to volume ratio, flow passages of CO₂ are sufficient to keep acceptable pressure drop, hence the system performance is similar when using TFM and PFM. We conclude that the flow splitting strategy is necessary for $W_{net} > 100$ MWe, but not recommended only at very small power capacity such as $W_{net} < 100$ MWe. Our work is important to understand the distinct feature of sCO₂ cycle driven by different heat sources.

1. Introduction

Supercritical carbon dioxide cycle (sCO₂ cycle) refers to a thermal cycle with supercritical CO₂ consecutively flowing through various components such as heater, turbine, cooler and compressor to convert thermal energy into mechanical power. Compared with conventional water-steam Rankine cycle, sCO₂ cycle has been shown to have higher efficiency, compact size and fast response to external load variation [1]. Various heat sources such as fossil energy, nuclear energy, solar energy, and waste heat can drive sCO₂ cycle for power generation [2,3]. Feher [4] proposed the sCO₂ Brayton cycle, including a compressor, a heater, a turbine and a cooler. The cycle is too simple thus the efficiency is low. On the basis of the Brayton cycle, recompression cycle (RC) was proposed by adding an additional flow branch. The major CO₂ flow stream

dissipates extra heat of the cycle to environment, but the additional flow branch is compressed without dissipating heat to environment. Thus, two compressors, instead of one, supply CO₂ flow rate, and two regenerative heat exchangers recycle heat in the system. RC is shown to have higher efficiency than the simple Brayton cycle [5]. RC is suitable for solar energy and nuclear energy, due to narrow temperature range of heat carrier fluid of heat source coupling with cycle [5–8]. The problem becomes complicated for sCO₂ cycle driven by fossil energy. Key issues are commented as follows.

1.1. Pressure drop penalty effect

The cycling mass flow rate m is scaled as $m = Q/\Delta h$, where Q is the heat absorption and Δh is the enthalpy difference of working fluid entering and leaving a boiler. Because CO₂ has much smaller Δh than

* Corresponding author at: Beijing Key Laboratory of Multiphase Flow and Heat Transfer for Low Grade Energy Utilization, North China Electric Power University, Beijing 102206, China.

E-mail address: xjl@ncepu.edu.cn (J. Xu).

<https://doi.org/10.1016/j.enconman.2020.113505>

Received 29 July 2020; Received in revised form 2 October 2020; Accepted 3 October 2020

0196-8904/© 2020 Elsevier Ltd. All rights reserved.

Nomenclature	
A	area, m ²
d	diameter, mm
e	exergy per unit mass, kJ/kg
E	exergy, MW
f	friction coefficient
G	mass flux, kg/m ² s
h	enthalpy per unit mass, kJ/kg
H	height, m
i	exergy destruction per unit mass, kJ/kg
I	exergy destruction, MW
L	length, m
m	mass flow rate, kg/s
n	number of tube rows in a heat exchanger module
P	pressure, MPa
q	thermal load of furnace, kW/m ³ or MW/m ² ; heat absorption per unit mass flow rate, kJ/kg; heat loss percentage of boiler, %
Q	thermal load, MW; heating value of coal, kJ/kg
Re	Reynolds number
s	entropy per unit mass, kJ/kg; tube pitch, mm
S	perimeter, m
T	temperature, °C
V	volume, m ³
w	output/ input work per unit mass, kJ/kg
w_x or w_y	furnace width or depth, m
W	output/ input work, MW
x	split ratio from the total mass flow rate
<i>Greek symbols</i>	
α	excess air coefficient
δ	tube wall thickness, mm; deviation temperature of flue gas in overlap zone, °C
ε	residual error
Δ	absolute roughness of internal tube wall, mm
ΔP	pressure drop, MPa
ΔT	temperature difference, °C
φ	non-uniformity coefficient of heat flux
η	efficiency
η_{th}	thermal efficiency
η_{ex}	exergy efficiency
ρ	density, kg/m ³
ϕ	boiler heat retention coefficient
τ	residence time
μ	dynamic viscosity, Pa·s
<i>Subscripts</i>	
0	environment state
1, 2, 3...	1b, 2b, 3b... state points of cycle
a	acceleration
A	cross-section area
ave	average
b	boiler
bv	volume of burning-out zone
c	cross-section
ex	exhaust
f	friction; fluid
fe	furnace exit
fire	combustion fire
fg	flue gas
flame	theoretical combustion
g	gravity or entropy generation
i	inner wall of tube; inlet of a component or flue gas region
in	input to the system
l	limit
o	outer wall of tube; outlet of a component or flue gas region
op	optimal
s	isentropic
v	furnace volume
w	tube wall
x, y, z	coordinates
<i>Abbreviations</i>	
AP	air preheater
C1, C3	main compressor
C2, C4	auxiliary compressor
EAP	external air preheater
HRH	high temperature reheater
HTR	high temperature regenerative heat exchanger
LHV	lower heating value
LRH	low temperature reheater
LTR	low temperature regenerative heat exchanger
PFM	partial flow mode
SH	superheater in upper furnace
T1, T3	high pressure turbine
T2, T4	low pressure turbine
TFM	total flow mode

water-steam under similar condition, m is significantly large, causing extremely large boiler pressure drop to decrease system efficiency, which is called the pressure drop penalty effect. To overcome this issue, the partial flow strategy is proposed to yield boiler module design [9]. Both flow rate and length for each module are cut to be half, reducing pressure drop to 1/8 of that with the total flow mode. It is shown that the pressure drop of CO₂ boiler can be equivalent to or smaller than the supercritical water-steam boiler.

1.2. Flue gas energy absorption over entire temperature range

sCO₂ cycle is suitable for high temperature heat source such as higher than ~550 °C [1]. However, flue gas in a coal fired boiler covers a very wide temperature range such as from ~1500 °C for combustion flame to 120 °C for exhaust flue gas. A single sCO₂ cycle is difficult to recover flue gas energy over entire temperature range. Thus, the cascade energy utilization is applied to deal with this issue [10]. In principle, flue gas energies in high, moderate and low temperature levels are extracted by a

top cycle, a bottom cycle and an air preheater, respectively. A criterion linking top cycle, bottom cycle and air preheater is presented [10].

For combined cycle, a bottom cycle usually works under lower temperature condition than a top cycle, resulting in an efficiency gap between the two cycles. Continued from the cascade energy utilization, an overlap energy utilization strategy was proposed to fill the efficiency gap between top cycle and bottom cycle [11]. The central idea is to set an overlap region in high temperature flue gas side. The flue gas energy in such an overlap region is not only absorbed by top cycle, but also by bottom cycle. In such a way, the bottom cycle efficiency is raised. The limit condition can be reached when the top cycle and the bottom cycle share identical efficiencies. Thus, the whole system efficiency is improved. Besides, when CO₂ is used instead of water, the temperature distribution of various heat transfer surfaces such as cooling wall, superheater and reheater will be changed. In turn, these changes may influence the combustion characteristics of sCO₂ boiler, which shall satisfy the ultra-low emission criterion of SO_x and NO_x etc [12].

We note that few works have been done on the effect of pressure

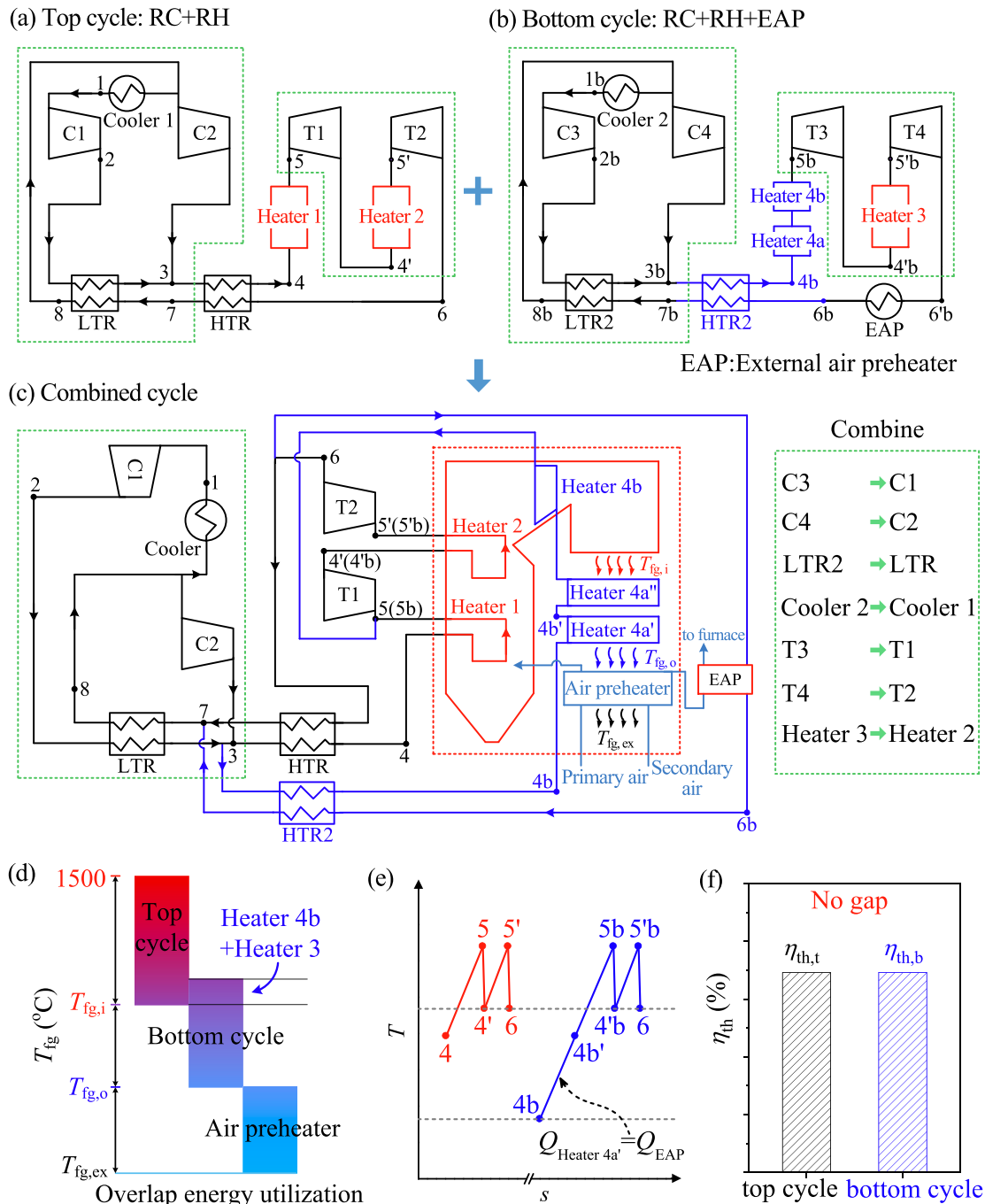


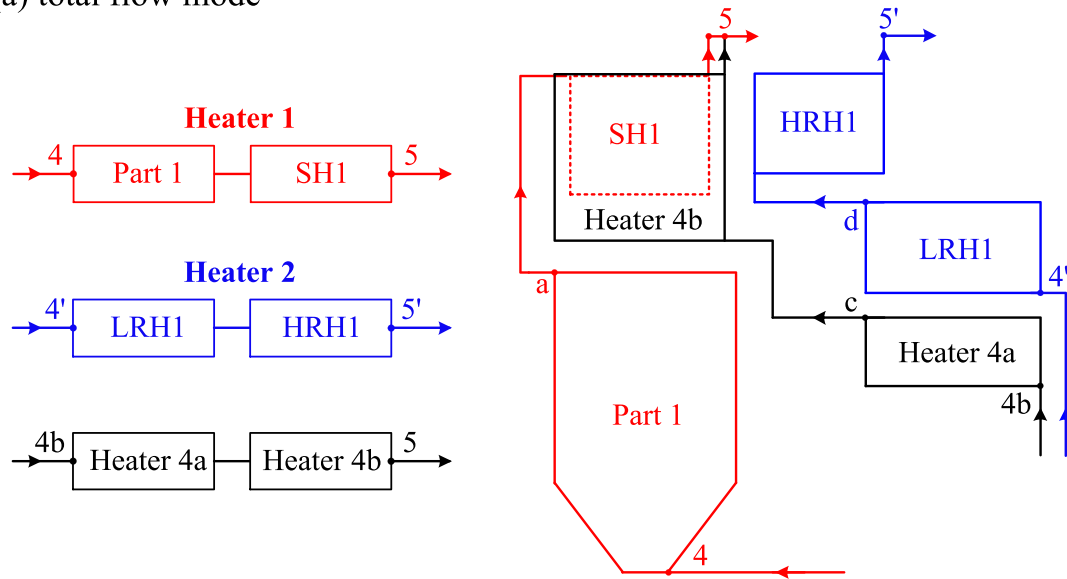
Fig. 1. sCO₂ cycle based on overlap energy utilization (a: top cycle; b: bottom cycle; c: combined cycle after components sharing; d: overlap energy utilization; e: T-s curves in boilers and turbines; f: no efficiency gap for overlap energy utilization).

drops of boilers on system performance. Electric Power Research Institute (EPRI, USA) noted the challenge of pressure drop caused by ultra-large flow rate for sCO₂ boiler, and considered using larger tube diameters to reduce pressure drop without exploring further solutions [13]. Moullec [14] designed a sCO₂ boiler for a power plant with its power capacity of 1000 MWe. To reduce pressure drops, the tube diameters of main heater, first and second reheating heaters attained 50 mm, 70 mm and 70 mm, respectively. In a design of 300 MWe capacity power plant, Yang et al. [15] used $d_i = 80$ mm and $n = 172$ for cooling wall tubes, and $d_i = 78$ mm and $n = 412$ for reheater tubes. Zhou et al [16] concluded that the combination of partial flow, flow symmetry and boiler local expansion strategy was useful to obtain lower pressure drop and wall temperature. For practical applications, it is not acceptable to

use large size tubes such as $d_i > 50$ mm. Currently, heat transfer data of sCO₂ in large diameter tubes are not available to support the boiler design [17,18]. For high pressure vessel design, the usage of large size tubes needs very thick tube walls, hence the thermal conductivity resistance of tube walls increases. Heat transfer coefficients significantly decrease when using very large diameter tubes.

We emphasized that the above works have been done for 1000 MWe coal fired power plant, belonging to large scale utilization. Currently, the 1000 MWe power plant is commercialized for supercritical watersteam Rankine cycle [19], which is almost the largest capacity in electricity market. An alternative way is to develop distributed energy system, which can use sCO₂ cycle to convert thermal energy into power. For distributed energy system using renewable energy such as solar or wind,

(a) total flow mode



(b) partial flow mode

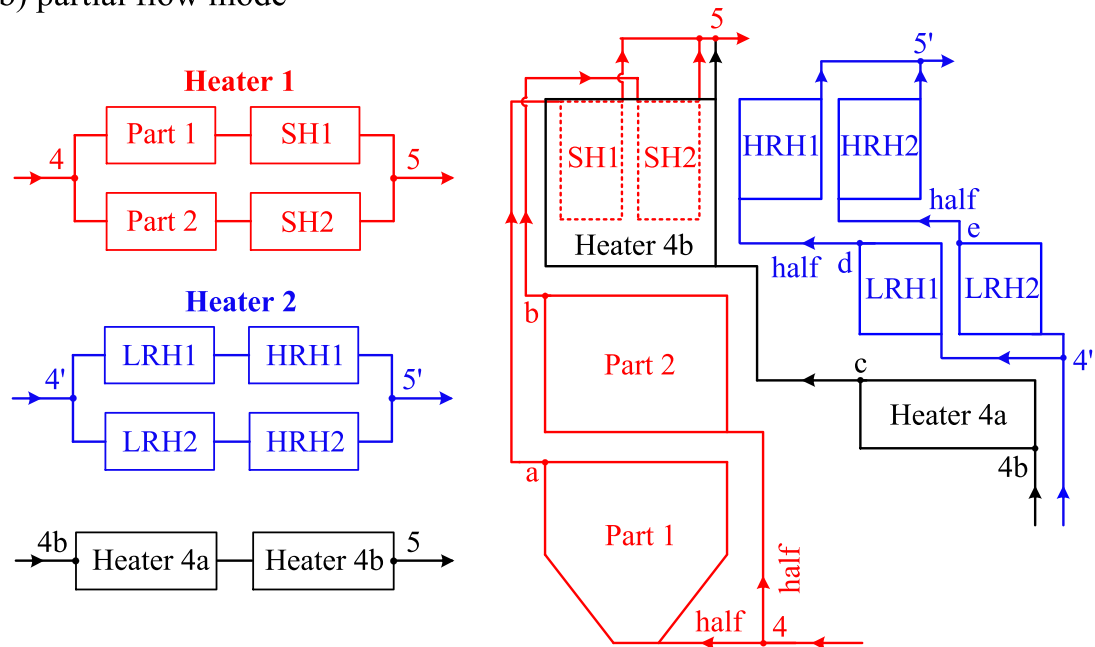


Fig. 2. The total flow mode (TFM) and partial flow mode (PFM) adapted to the boiler design.

the power capacity can be in the range of 10–100 MWe [20]. However, it is difficult to construct coal fired power plant with very small capacity such as 10 MWe. Under such circumstance, the combustion fire may directly contact heater surface to form coke or slagging on cooling wall tubes. Thus, the power capacities investigated in this paper are in the range of 50–1000 MWe.

Because the system performance is determined by the coupling between thermodynamics and energy transfer and conversion process, the performance may not be the same at different power capacities. Now that the 1000 MWe sCO₂ coal fired power plant has been analyzed, one may ask questions such as: (i) Can the 1000 MWe capacity results be directly used for smaller capacity design? (ii) How does the power capacity influence the system performance?

The present paper tries to answer the above questions. Specially, the pressure drop penalty effect is paid great attention. In order to do that, comparative studies are performed between using total flow mode

(TFM) and partial flow mode (PFM). Totally, eleven power capacities are investigated in the range of 50–1000 MWe. Different power capacities correspond to different geometry parameters of sCO₂ boiler. Hence, the ratio of surface area to volume of sCO₂ boiler is changed. This parameter changes the number of tubes to determine mass flux in cooling wall tubes, which is the key to dominate pressure drops in sCO₂ boiler. The important conclusion is that, when power capacities decrease, mass fluxes in cooling wall tubes are reduced. Hence, the pressure drop penalty effect is weakened. When the power capacity is reduced to 100 MWe, the pressure drop penalty effect is weak, under which TFM is sufficient. However, PFM is necessary for capacities larger than 100 MWe. The present paper is organized as follows. Section 2 describes sCO₂ cycle and boiler design. Section 3 deals with the numerical model coupling sCO₂ cycle with boiler. Section 4 reports main results and discussion. Major conclusions are summarized in Section 5.

Now that the partial flow strategy has been proposed for sCO₂ coal

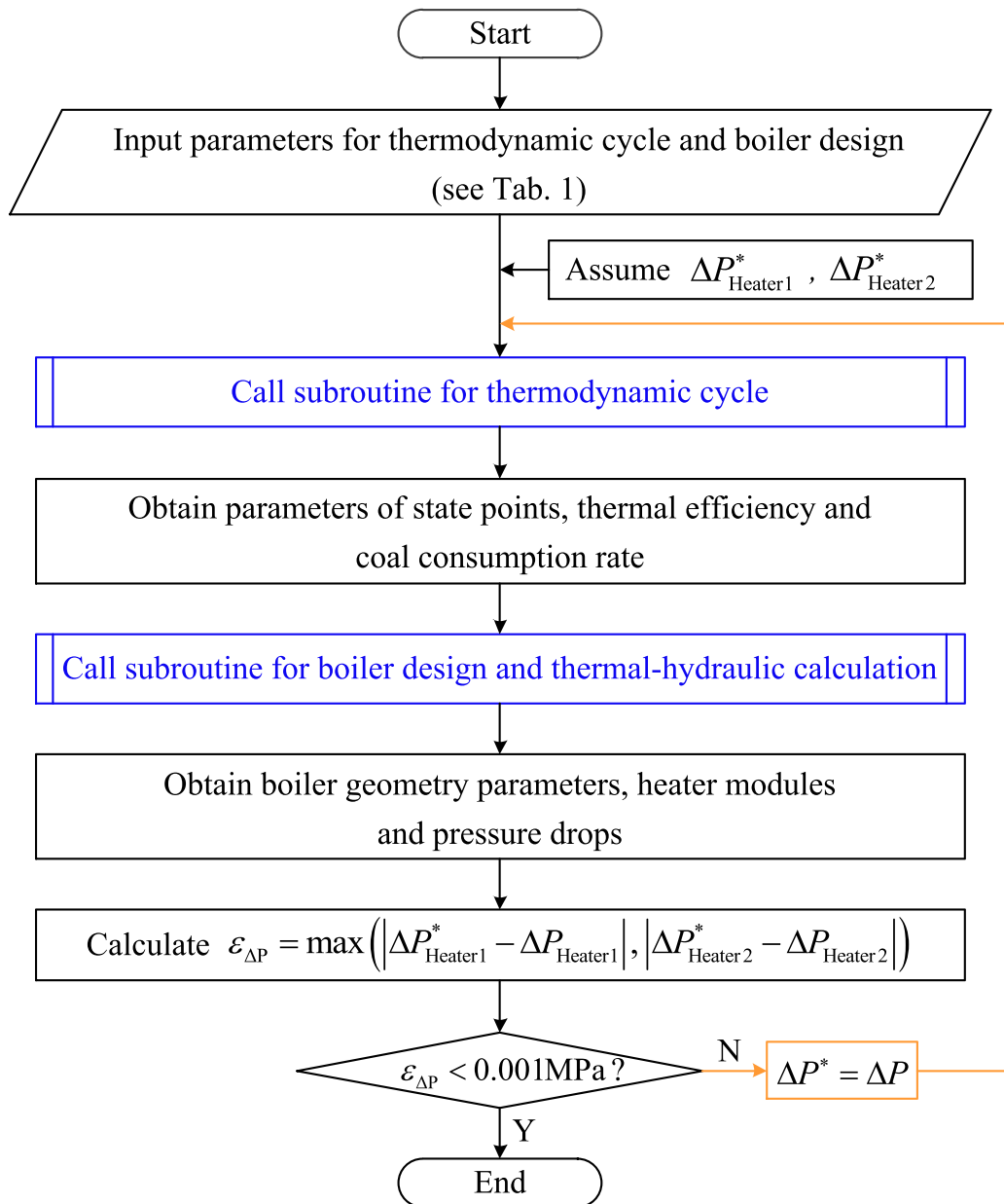


Fig. 3. Implement of numerical calculations for cycle coupling with boiler.

fired power plant [9], we highlight new findings of the present paper here. First, Ref. [9] studied the sCO₂ coal fired power plant at a fixed power capacity of $W_{\text{net}} = 1000$ MWe. The present paper investigated the sCO₂ power plant covering the range of $W_{\text{net}} = 50\text{--}1000$ MWe. We conclude that the partial flow strategy is necessary for $W_{\text{net}} > 100$ MWe, but not necessary for very small power plant such as $W_{\text{net}} < 100$ MWe, under which the surface area to volume ratio of the boiler is sufficient to keep reasonable mass flux to weaken the pressure drop penalty effect. Second, the scale laws regarding boiler characteristics parameters against power capacities are theoretically established. It is found that the theoretically developed scale laws match numerical simulations well. Third, compared to our previous work, an improved mathematical model coupling the thermodynamic analysis and thermal-hydraulic characteristics of boilers is established.

2. sCO₂ cycle coupling with boiler

2.1. sCO₂ cycle incorporating overlap energy utilization

Modified from Ref. [11], the sCO₂ cycle is shown in Fig. 1. The combined cycle, components sharing and overlap energy utilization are comprehensively applied, which are described as follows:

2.1.1. The combined cycle

The top cycle applies recompression cycle plus reheating, represented by RC + RH (see Fig. 1a). Heaters 1 and 2 are the heat sources to drive the cycle. C1 and C2 are the two compressors, and T1 and T2 are the two turbines. HTR and LTR are the two regenerative heat exchangers, operating at high and low temperature ranges respectively to recycle heat in the system. Cooler 1 dissipates extra heat to environment. The bottom cycle shown in Fig. 1b is similar to Fig. 1a, but an external air preheater (EAP) recycles extra heat of bottom cycle to the boiler. Heaters 4a, 4b and 3 are the heat sources to drive the bottom cycle.

2.1.2. Components sharing

Even though the CO₂ flow rates in specific components are different for top cycle and bottom cycle, the CO₂ pressures and temperatures in these components of the two cycles are similar. Thus, the components sharing technique is applied to simplify the system layout. For example, C3 in bottom cycle is combined into C1 in top cycle, thus C3 is not shown in Fig. 1c. Similar components sharing technique is also applied to C4, LTR2, Cooler 2, T3, T4 and Heater 3. The combined cycle, after the components sharing, is shown in Fig. 1c. Due to the components sharing, the points of 5b, 4'b and 5'b coincide with 5, 4', 5' respectively.

2.1.3. Overlap energy utilization

The overlap energy utilization is shown in Fig. 1d. The three regions of flue gas energies correspond to the temperature ranges of 1500 °C- $T_{fg,i}$, $T_{fg,i}$ - $T_{fg,o}$ and $T_{fg,o}$ - $T_{fg,ex}$. Thus, $T_{fg,i}$, $T_{fg,o}$ and $T_{fg,ex}$ are called the interface temperatures among the three regions. An overlap zone is set in high temperature region, covering the flue gas temperature range from $T_{fg,i} + \delta$ to $T_{fg,i}$, where δ is called the deviation temperature. Flue gas energies in this subzone is not only absorbed by top cycle, but also by bottom cycle, represented by Heater 4b and Heater 3. For practical cycle design, Heater 3 is embedded in Heater 2. Fig. 1e shows the T - s roadmaps for heat absorption and expansion processes, in which red color represents the top cycle, and blue color represents the bottom cycle. For bottom cycle, the heat absorption process 4b-5b consists of two components: one is 4b-4b' and the other is 4b'-5b. Due to the heat recycling by EAP, the heat absorption process 4b-4b' is compensated by the heat recycling of EAP. Hence, the real heat absorption process is 4b'-5b, which repeats the process 4-5 in top cycle. Similarly, the expansion processes in the two cycles are repeated. The overlap energy utilization ensures no efficiency gap between top cycle and bottom cycle (see Fig. 1f).

2.2. The sCO₂ boiler

Fig. 1c shows the sCO₂ cycle driven by Heaters 1, 2, 4a and 4b, which should be adapted to a boiler. Here, we deal with indirect sCO₂ cycle, in which combustion takes place in a furnace but CO₂ flows in tubes. Flue gas in furnace and CO₂ in tubes are separated by tube walls of a π -type pulverized coal boiler. To identify the pressure drop penalty effect, comparative investigations were performed for total flow mode (TFM) and partial flow mode (PFM). The former can be easily implemented in a boiler, which is similar to a conventional water-steam boiler (see Fig. 2a). Heaters are classified as radiation heat transfer surface and convective heat transfer surface [21]. A heater in a furnace belongs to radiation heat transfer surface, while a heater in horizontal flue or tail flue belongs to convective heat transfer surface. TFM is a series connection mode, with total CO₂ flow rate consecutively flowing through each component. To arrange heaters in a boiler, Heater 1 in Fig. 1c is decoupled into Part 1 and SH1 as the main heating process, in which Part 1 is a cooling wall module at lower part of furnace and SH1 is a superheating heater module suspended in the top of furnace. Heater 2 is decoupled into LRH1 and HRH1 as the reheating process. Both Heaters 1 and 2 supply thermal loads to the top cycle, and Heater 2 also supplies heat to the bottom cycle. Heaters 4a and 4b are connected with each other, providing heat loads to the bottom cycle. Part 1, Heater 4b and SH1 are arranged as the radiation heat sources, and others are the convective heat sources (see Fig. 2a).

PFM is a parallel connection mode (see Fig. 2b). The total flow rate, for example at point 4, is divided into two parallel lines, each line accounts for half flow rate. Because frictional pressure drop is scaled as $\Delta P_f \sim m^2$, ΔP_f decreases to 1/4 of that for TFM. One notes that PFM needs more heater modules to decrease module length. For flow length cut to be half, ΔP_f is $\sim 1/8$ of that for TFM. Thus, PFM is called the 1/8 pressure drop reduction technique. In Fig. 2b, Heaters 1 and 2 are subdivided into eight modules. A boiler adapting to PFM behaves module design feature.

Table 1

Parameters for the cycle computations and boiler design.

Parameters	Values
Cycle type	Indirect
Combustion type	Pulverized coal boiler
Net power (W_{net})	50–1000 MWe
Turbine inlet temperature (T_5 , $T_{5'}$)	620 °C
Turbine T1 inlet pressure (P_5)	30 MPa
Compressor C1 inlet temperature (T_1)	32 °C
Compressor C1 inlet pressure (P_1)	7.6 MPa
Pressure drop in LTR/HTR/HTR2(ΔP)	0.1 MPa
Pinch temperature difference in LTR/HTR(ΔT_{LTR} , ΔT_{HTR})	10 °C
Turbines isentropic efficiency ($\eta_{t,s}$)	0.93
Compressors isentropic efficiency ($\eta_{c,s}$)	0.89
Exhaust gas temperature ($T_{fg,ex}$)	123 °C
Environment temperature (T_0)	20 °C
Excess air coefficient (α)	1.2
Primary air temperature entering air preheater	31 °C
Primary air temperature entering furnace	320 °C
Ratio of primary air flow rate to the total air flow rate	0.19
Secondary air temperature entering air preheater	23 °C
Ratio of secondary air flow rate to the total air flow rate	0.81
Ash hopper angle	55°
Pinch temperature different between flue gas and CO ₂ at point 4' (ΔT_4)	40 °C
Pinch temperature different between flue gas and CO ₂ at point 4b (ΔT_{4b})	30 °C

3. Numerical model

Fig. 3 shows the computation scheme. The numerical model is suitable for various power capacities. Following procedures are applied: (i) Input parameters for a referenced cycle and boiler design, see Table 1 for necessary parameters. (ii) Pressure drops in Heaters 1 and 2 are assumed. (iii) Call thermodynamic cycle subroutine. (iv) Obtain parameters at various state points, thermal efficiency and coal consumption rate. (v) Call sCO₂ boiler subroutine. (vi) Update geometry parameters and thermal-hydraulic parameters of boiler. (vii) Calculate residual value of pressure drops in Heaters 1 and 2. (viii) If the residual value is smaller than a setting value, the computation is stopped. Otherwise, the above procedures are repeated.

One notes that a power plant is a very complicated system, whose performance is influenced by many factors. Here, the pressure drop penalty effect is emphasized. Following assumptions are made: (i) steady system operation; (ii) isentropic efficiencies are 0.89 for compressors and 0.93 for turbines [7,22,23], which are not changed for different power capacities. (iii) Pinch temperatures are 10 °C in regenerative heat exchangers such as LTR and HTR. (iv) There are several mixing points in the cycle. No mixing-induced exergy destruction exists due to the same temperatures and pressures for mixing of different fluid streams. (v) There is no flow rate deviation among different tubes in various heaters.

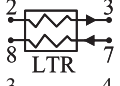
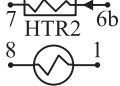
Power generation efficiency is important to characterize a power plant performance, which is the outcome of thermal efficiency timing other efficiency components such as pipeline efficiency and generator efficiency, etc [24]. Because we focus on the analysis of pressure drop penalty effect, the comparison of thermal efficiency at various conditions is sufficient.

3.1. Computation of sCO₂ cycle

The top cycle and bottom cycle are overlapped to a single cycle (see Fig. 1c). The total CO₂ flow rate splits into two streams, with one stream flowing through Heater 1 and the other stream flowing through Heaters 4a and 4b. The ratio of flow rate in Heaters 4a and 4b to the total flow rate is defined as $x_{Heater 4}$, linking the heat transfer from flue gas to CO₂ of the cycle.

In flue gas side, thermal load Q is

Table 2
Equations for components in the cycle.

Components	Equations and exergy destructions
	$\eta_{e,s} = \frac{h_{2s} - h_1}{h_2 - h_1}, w_{C1} = (1 - x_{C2})(h_2 - h_1); i_{C1} = w_{C1} - (1 - x_{C2})(e_2 - e_1)$
	$\eta_{e,s} = \frac{h_{3s} - h_8}{h_3 - h_8}, w_{C2} = x_{C2}(h_3 - h_8); i_{C2} = w_{C2} - x_{C2}(e_3 - e_8)$
	$\eta_{t,s} = \frac{h_5 - h_{4'}}{h_5 - h_{4's}}, w_{T1} = h_5 - h_{4'}; i_{T1} = e_5 - e_{4'} - w_{T1}$
	$P_{5'} = \sqrt{P_5 P_6}, \eta_{t,s} = \frac{h_{5'} - h_6}{h_{5'} - h_{6s}}, w_{T2} = h_{5'} - h_6; i_{T2} = e_{5'} - e_6 - w_{T2}$
	$T_8 = T_2 + \Delta T_{LTR}, x_{C2} = 1 - \frac{h_7 - h_8}{h_3 - h_2}; i_{LTR} = e_7 - e_8 - (1 - x_{C2})(e_3 - e_2)$
	$T_7 = T_3 + \Delta T_{HTR}, (1 - x_{EAP})(h_6 - h_7) = (1 - x_{Heater\ 4})(h_4 - h_3); i_{HTR} = (1 - x_{EAP})(e_6 - e_7) - (1 - x_{Heater\ 4})(e_4 - e_3)$
	$x_{EAP}(h_{6b} - h_7) = x_{Heater\ 4}(h_{4b} - h_3); i_{HTR2} = x_{EAP}(e_{6b} - e_7) - x_{Heater\ 4}(e_{4b} - e_3)$
	$i_{Cooler} = (1 - x_{C2})(e_8 - e_1)$

$$Q = Q_{Heater\ 1} + Q_{Heater\ 2} + Q_{Heater\ 4b} + Q_{Heater\ 4a} + Q_{AP} \quad (1)$$

Because $T_{fg,i}$, $T_{fg,o}$ and $T_{fg,ex}$ are the three interface temperatures of flue gas, thermal loads in Eq. (1) are decoupled as

$$\begin{cases} Q_{Heater\ 1} + Q_{Heater\ 2} + Q_{Heater\ 4b} = \phi m_{coal}(h_{flame} - h_{fg,i}) & \text{high temperature region} \\ Q_{Heater\ 4a} = \phi m_{coal}(h_{fg,i} - h_{fg,o}) & \text{moderate temperature region} \\ Q_{AP} = \phi m_{coal}(h_{fg,o} - h_{fg,ex}) & \text{low temperature region} \end{cases} \quad (2)$$

where h is the flue gas enthalpy, ϕ is the boiler heat retention coefficient, $\phi = 1 - q_5/(100\eta_b + q_5)$, η_b is the boiler efficiency and q_5 is one component of heat loss of boiler to environment, which can be determined by Ref. [21]. The coal consumption rate is

$$m_{coal} = \frac{q_{total} m_{CO_2}}{\eta_b Q_{LHV}} \quad (3)$$

where q_{total} is the heat absorption per unit mass flow rate of CO_2 , m_{CO_2} is the total mass flow rate of CO_2 , Q_{LHV} is the low heating value of coal per unit mass.

In CO_2 side, $Q_{Heater\ 4a}$ is

$$Q_{Heater\ 4a} = x_{Heater\ 4} m_{CO_2} (h_{4'} - h_{4b}) \quad (4)$$

The flue gas temperatures $T_{fg,i}$ and $T_{fg,o}$ have the relationship with the CO_2 temperature as

$$T_{fg,i} = T_{4'} + \Delta T_{4'}, T_{fg,o} = T_{4b} + \Delta T_{4b} \quad (5)$$

where $\Delta T_{4'}$ and ΔT_{4b} are the pinch temperatures of heat exchangers, which are $40^\circ C$ and $30^\circ C$ respectively (see Table 1). In Eqs. (4) and (5), $T_{4'}$ and T_{4b} are the temperatures at the outlet and inlet of Heater 4a. The iteration of computations is stopped when $Q_{Heater\ 4a}$ determined by Eq. (2) equals to that determined by Eq. (4).

Table 3
Properties of the designed coal.

C_{ar}	H_{ar}	O_{ar}	N_{ar}	S_{ar}	A_{ar}	M_{ar}	V_{daf}	Q_{LHV}
61.70	3.67	8.56	1.12	0.60	8.80	15.55	34.73	23,442

C (carbon), H (hydrogen), O (oxygen), N (nitrogen), S (sulfur), A (ash), M (moisture), V (volatile).
Subscripts ar, d, af mean as received, dry and ash free, $C_{ar} + H_{ar} + O_{ar} + N_{ar} + S_{ar} + A_{ar} + M_{ar} = 100$.

Once thermodynamic parameters at various state points are obtained (see Table 2), w_{net} (net power per unit mass flow rate of CO_2), q_{total} and η_{th} (thermal efficiency) are

$$w_{net} = (w_{T1} + w_{T2}) - (w_{C1} + w_{C2}) \quad (6)$$

$$q_{total} = (1 - x_{Heater\ 4})(h_5 - h_4) + x_{Heater\ 4}(h_5 - h_{4b}) + (h_5 - h_{4'}) - x_{EAP}(h_6 - h_{6b}) \quad (7)$$

$$\eta_{th} = \frac{w_{net}}{q_{total}} \quad (8)$$

Then, m_{CO_2} is

$$m_{CO_2} = \frac{W_{net}}{w_{net}} \quad (9)$$

where W_{net} is the power capacity (net power output), which is in the range of 50–1000 MWe. Specific exergy per unit mass flow rate is $e = h - T_0 s$, and exergy destruction is the difference between input exergy and output exergy (see Table 2) [25]. Exergy efficiency of the system is

$$\eta_{ex} = \frac{W_{net}}{E_{in}} \quad (10)$$

The input exergy of system E_{in} equals to the chemical exergy of coal [26]

$$E_{in} = m_{coal} Q_{LHV} \left(1.0064 + 0.1519 \frac{H_{ar}}{C_{ar}} + 0.0616 \frac{O_{ar}}{C_{ar}} + 0.0429 \frac{N_{ar}}{C_{ar}} \right) \quad (11)$$

where C_{ar} , H_{ar} , O_{ar} and N_{ar} are the ratios of C (carbon), H (hydrogen), O (oxygen) and N (nitrogen) on the as-received basis of designed coal, respectively (see Table 3). Considering boiler as a whole component, the exergy output (E_b) and exergy loss per unit mass flow rate (I_b) are

$$E_b = m_{CO_2} [(1 - x_{Heater\ 4})(e_5 - e_4) + x_{Heater\ 4}(e_5 - e_{4b}) + (e_{5'} - e_{4'})] \quad (12)$$

$$I_b = E_{in} + m_{CO_2} x_{EAP}(e_6 - e_{6b}) - E_b \quad (13)$$

The exergy loss in component j (I_j) and total exergy loss (I_{total}) are

$$I_j = m_j i_j, I_{total} = \sum I_j \quad (14)$$

Fig. A1 in appendix shows the computation scheme of thermodynamic cycle.

3.2. Computation of sCO_2 boiler

Fig. A2 in appendix shows the computation scheme of sCO_2 boiler and its thermal-hydraulic characteristic. The boiler model shown in Fig. 4 represents the main furnace structure, not including tail flue

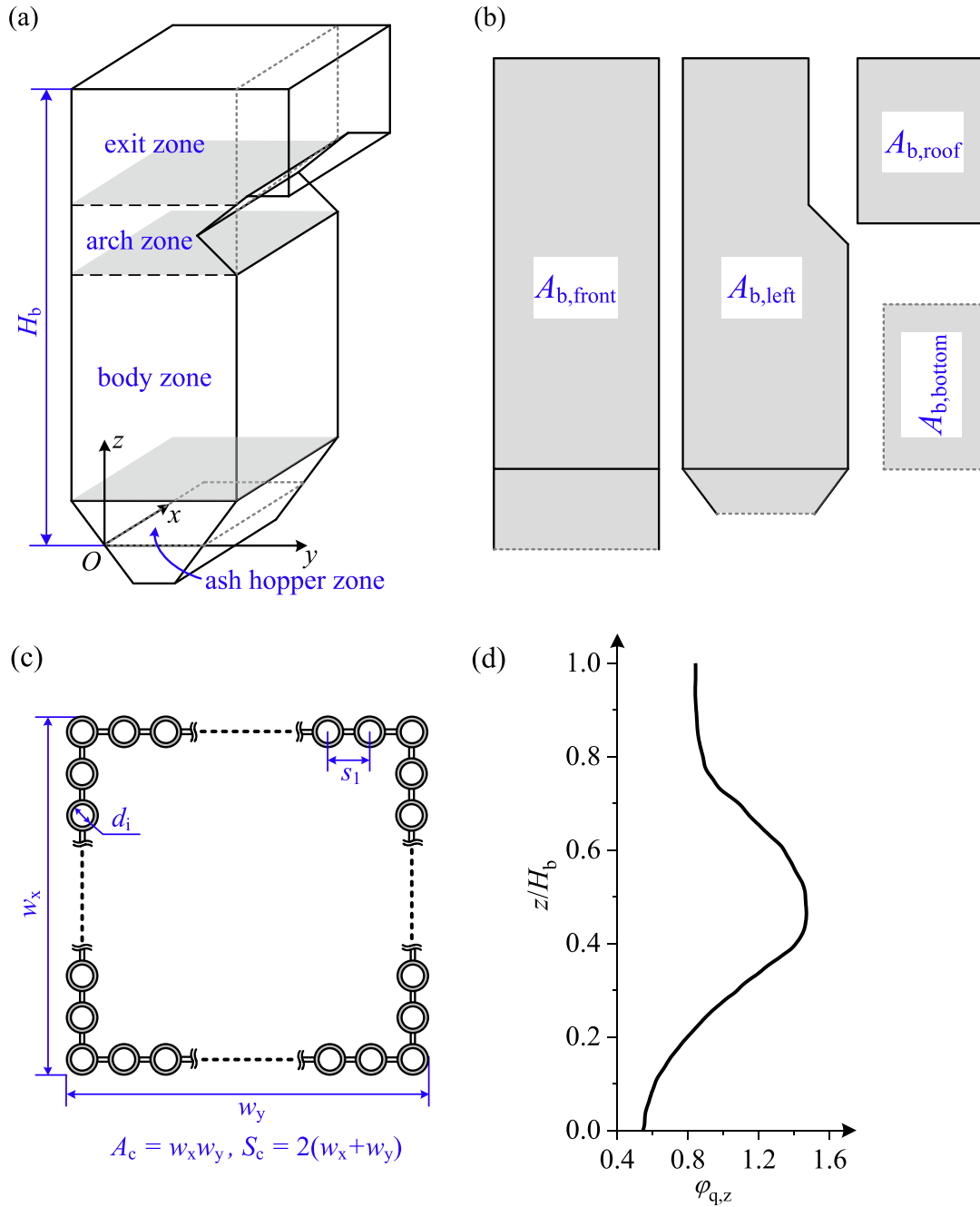


Fig. 4. The furnace model (a: 3D furnace; b: heat transfer surfaces of front wall, left wall, roof wall and bottom wall; c: cross-section of furnace; d: heat load distribution along furnace height).

volume. Four regions including an ash hopper zone, a body zone, an arch zone and an exit zone are arranged, from furnace bottom to top. An original point O for the x - y - z coordinate is located at the center height of the ash hopper. The furnace height is H_b , starting from the original point O to the furnace roof. The cross-section is $w_x \times w_y$, having $w_x = w_y$ for square cross-section. The furnace volume V_b is the sum of the four zones. The surface areas are $A_{b,front}$ for front wall, $A_{b,back}$ for back wall, $A_{b,left}$ for left wall, $A_{b,right}$ for right wall, $A_{b,roof}$ for roof wall, and $A_{b,bottom}$ for bottom wall, respectively. The whole surface area of furnace walls (A_b) is the sum of the above.

For sCO_2 boiler, the thermal-hydraulic characteristics of CO_2 is quite different from that of water-steam boiler, thus the module boiler design is used (see Fig. 2), but there is mini difference in combustion side for the two kinds of boilers. We draw lessons from supercritical water-steam

boiler to design thermal loads of sCO_2 boiler, in which q_v and q_A are the two important parameters [21,27,28]. They refer to the volume heat flux and surface heat flux, respectively. Once having q_v and q_A , the geometry parameters of furnace are determined as

$$A_c = \frac{m_{coal} Q_{LHV}}{q_A}, V_b = \frac{m_{coal} Q_{LHV}}{q_v}, w_x = w_y = A_c^{0.5} \quad (15)$$

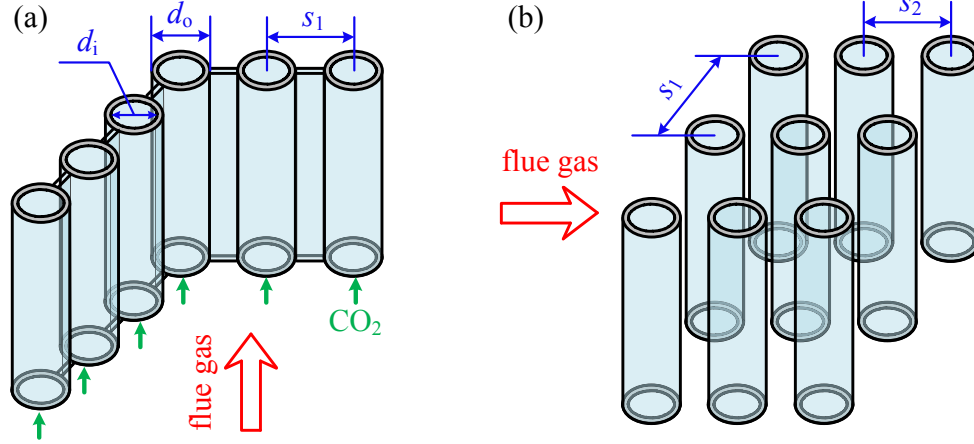
We note that different power capacities have different q_A and q_v , yielding different geometrical parameters of furnace. The average heat flux of furnace is

$$q_{ave} = \frac{Q_{Heater 1} + Q_{Heater 4b}}{A_b + A_{SH}} \quad (16)$$

Where A_{SH} is the surface area exposed in flue gas for superheater

Table 4
Geometrical parameters of heater modules of boiler (mm).

Heat exchange modules	$d_i \times \delta$	d_o	s_1	s_2
Part 1 or Part 2	24 × 8	40	56	–
Heater 4b	20 × 6	32	45	–
SH1 or SH2	32 × 8	48	1350	60
HRH	35 × 5	45	450	60
LRH	48 × 5.5	59	120	74



Tube arrangement and geometry parameters (a: cooling wall modules of Part 1, Part 2 and Heater 4b; b: other modules of SH1, SH2, HRH and LRH).

such as SH1 in Fig. 2a or SH1 and SH2 in Fig. 2b. By introducing non-uniform coefficient of heat flux distribution $\varphi_{q,z}$ (see Ref. [29] and Fig. 4d), the local heat flux at any z location is

$$q_z = q_{ave} \cdot \varphi_{q,z} \quad (17)$$

The parameter of q_{bv} , volume heat flux in burning-out zone, is written as [27]

$$q_{bv} = \frac{m_{coal} Q_{LHV}}{V_{bv}} \quad (18)$$

where V_{bv} is the volume of burning-out zone, covering the height from the top burners to the centerline of the arch zone. For practical operation, q_{bv} should be smaller than a limit value, which is in the range of 200–260 kW/m³ for water-steam boiler [27], under which coal is completely burned. Fig. 4d is further explained here. We note that cooling wall in furnace belongs to radiation heat transfer surface. Radiation heat transfer between a combustion fire temperature T_{fire} such as 1600 °C and a cooling wall temperature T_w such as 700 °C yields the heat flux q insensitive to the variation of T_w due to the scale law of $q \sim (T_{fire}^4 - T_w^4)$, noting the temperature unit of K.

The tube size of heater module is important to influence flow and heat transfer of CO₂. The inner diameter of cooling wall tubes (d_i) is in the range of 20–30 mm [21]. Larger d_i yields smaller pressure drop, but results in lower heat transfer coefficient. Because sCO₂ boiler operates at high pressure larger than 30 MPa, larger d_i increases wall thickness δ , increasing thermal conduction resistance of tube walls to further deteriorate heat transfer. As cooling wall modules, Part 1 and Part 2 use $d_i = 24$ mm with $\delta = 8$ mm. HRH and LRH are reheating modules, which can use larger tube sizes such as $d_i = 35$ mm for HRH and $d_i = 48$ mm for LRH (see Table 4).

Pressure drop in a module consists of frictional pressure drop ΔP_f , gravity pressure drop ΔP_g and acceleration pressure drop ΔP_a :

$$\Delta P = \Delta P_f + \Delta P_g + \Delta P_a \quad (19)$$

ΔP_a is only dependent on the outlet and inlet fluid states:

$$\Delta P_a = G^2 \left(\frac{1}{\rho_o} - \frac{1}{\rho_i} \right) \quad (20)$$

where ρ_o and ρ_i are the CO₂ densities at the module outlet and inlet, respectively, G is the mass flux. Because physical properties of CO₂ vary along heating length, the length of heater module is subdivided into many subsections, thus local fluid temperatures are used to characterize physical properties. ΔP_f and ΔP_g are the integration effects over whole module length:

$$\Delta P_f = \int_{\text{whole module length}} \frac{f \cdot G^2}{d_i \cdot 2\rho} dz, \quad (21)$$

$$\Delta P_g = \int_{\text{whole module length}} \rho g dz$$

Where g is the gravity acceleration. The friction factor f is calculated as [30]

$$f = \frac{1}{3.24lg^2 \left[\left(\frac{\Delta/d_i}{3.7} \right)^{1.11} + \frac{6.9}{Re} \right]} \quad (22)$$

where Δ is the absolute roughness of internal tube wall, which is 0.012 mm for stainless-steel tube [31]. The Reynolds number Re is

$$Re = \frac{Gd_i}{\mu} \quad (23)$$

where μ is the viscosity of CO₂, which is dependent on local temperature along flow length.

sCO₂ boiler includes both radiation modules and convective modules. The determination of thermal loads assigned to the two types of heat transfer modules needs to be iterated. Practically, an initial number of tube rows of SH1 for TFM or SH1 and SH2 for PFM is assigned. On one hand, the thermal load to the superheater, Q_{SH} , is determined due to the cycle requirement. On the other hand, it is determined by heat transfer from flue gas to CO₂. The iteration is stopped when difference between

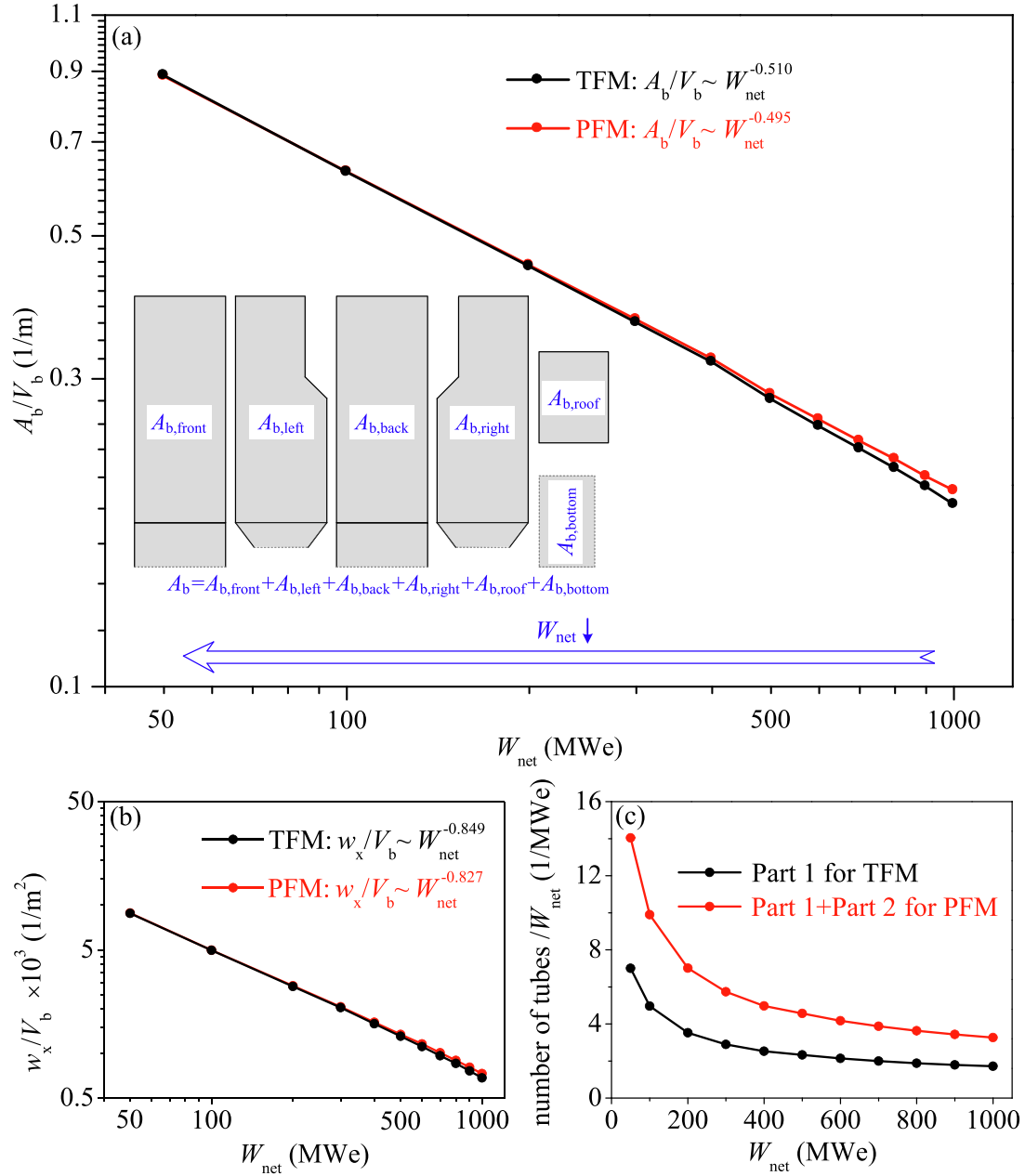


Fig. 5. The ratios of surface area to volume (a), width to volume (b) and number of tubes per unit power capacity (c) at different power capacities.

the two methods computation is smaller than an accepted residual value. The computation of convective heat transfer modules involves temperature difference between flue gas and CO₂, heat transfer coefficient, heat transfer area and pressure drop (see Fig. A2 in appendix). The equations for these computations are cited from Ref. [21].

4. Results and discussion

4.1. Scale law regarding power capacities

We give a scale law analysis regarding power capacities. Assigning L as the characteristic length of a furnace, the furnace volume and surface area are $V_b \sim L^3$ and $A_b \sim L^2$, respectively. The surface area to volume ratio and length to volume ratio are

$$\frac{A_b}{V_b} \sim L^{-1}, \quad \frac{L}{V_b} \sim L^{-2} \quad (24)$$

On the other hand, Equation (9) shows that

$$m \sim W_{net} \quad (25)$$

The total cross-section area of CO₂ in cooling wall tubes is

$$A_f = \frac{\pi d_i^2}{4} \times \frac{2(w_x + w_y)}{s_1} \sim L \quad (26)$$

where d_i is the inner tube diameter, s_1 is the distance between two neighboring tubes. The first and second terms of right side of Eq. (26) represent the single tube cross-section area and the number of tubes, respectively. Because d_i and s_1 are not changed at different W_{net} , A_f is scaled as $A_f \sim L$.

The relationship between L and W_{net} should be achieved. For constant volume heat flux q_v , L is scaled as

$$L \sim W_{net}^{1/3} \quad (27)$$

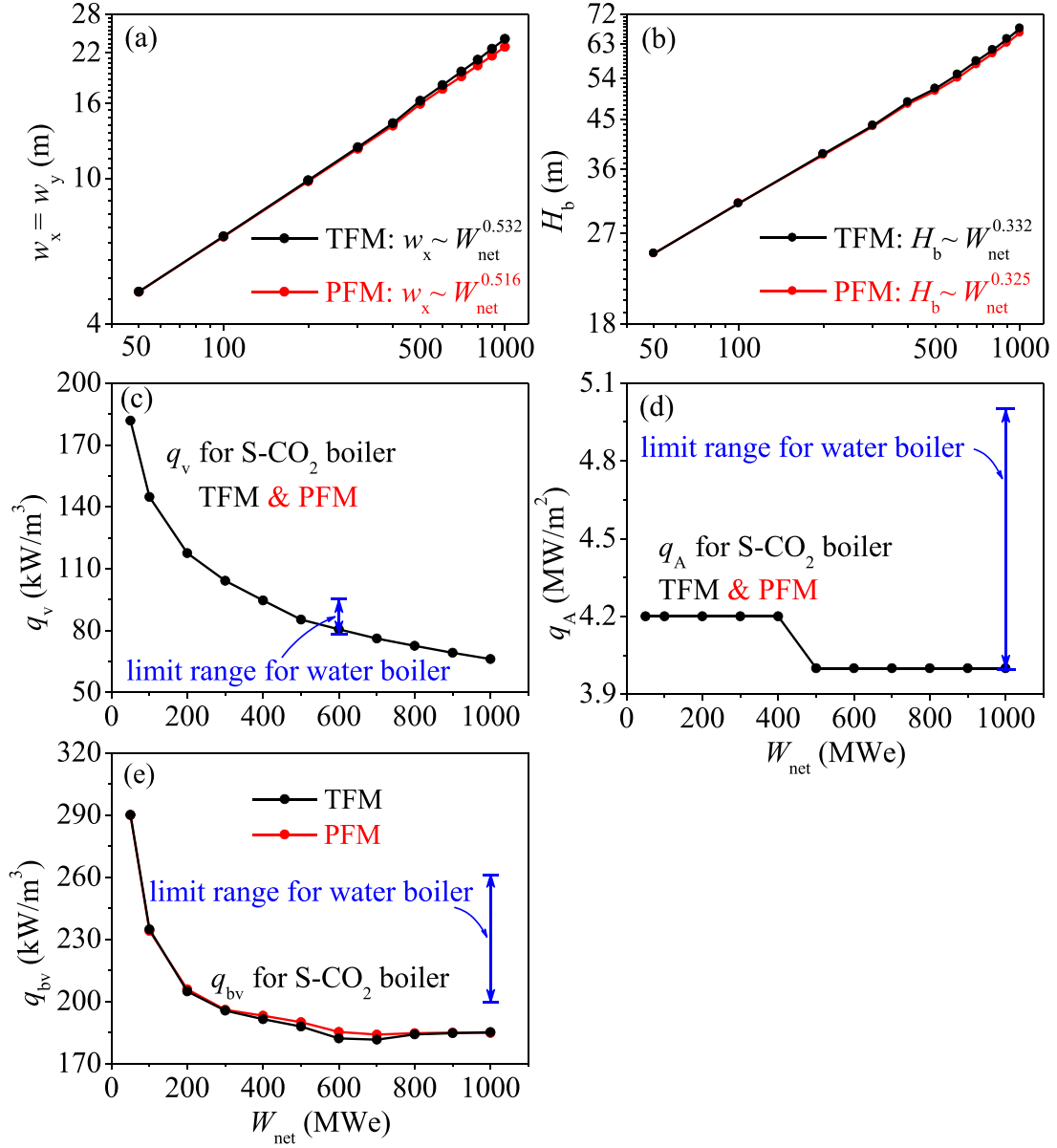


Fig. 6. Characteristic sizes and heat loads at different power capacities (a: furnace width; b: furnace height; c: q_v curve, a reference value is 80 ~ 95 kW/m³ for water-steam boiler at 600 MWe; d: q_A curve, a reference value is 4.0 ~ 5.0 MW/m² for water-steam boiler at 1000 MWe; e: q_{bv} curves, a reference value is 200 ~ 260 kW/m³ for water-steam boiler at 1000 MWe).

Alternatively, for constant surface heat flux q_A , L is scaled as

$$L \sim W_{\text{net}}^{1/2} \quad (28)$$

Equations (27) and (28) are combined to have

$$L \sim W_{\text{net}}^{1/3 \sim 1/2} \quad (29)$$

With the definition of $G = m/A_f$, combining Eqs. (25), (26) and (29) yields

$$G \sim W_{\text{net}}^{1/2 \sim 2/3} \quad (30)$$

Substituting Eq. (29) into Eq. (24) yields

$$\frac{A_b}{V_b} \sim W_{\text{net}}^{-(1/3 \sim 1/2)}, \quad \frac{L}{V_b} \sim W_{\text{net}}^{-(2/3 \sim 1)} \quad (31)$$

The scale law regarding frictional pressure drops is to be established. Assuming constant d_i and f , Eq. (21) shows that $\Delta P_f \sim G^2 L$, where L is the heater length. Substituting Eqs. (29) and (30) into this scale law

yields

$$\Delta P_f \sim W_{\text{net}}^{1.33 \sim 1.50} \quad (32)$$

Equation (32) shows the sharp increase of ΔP_f with increase of W_{net} . Neglecting the variation of physical properties, Eq. (21) is rewritten as

$$\Delta P_f = f \cdot \frac{L}{d_i} \cdot \frac{G^2}{2\rho} \quad (33)$$

For PFM, both G and L are cut to be half to those for TFM. Hence the following criterion is reached:

$$\Delta P_f|_{\text{PFM}} \approx \frac{1}{8} \Delta P_f|_{\text{TFM}} \quad (34)$$

Equation (34) is called the 1/8 pressure drop reduction criterion [9]. The objective of this paper is to examine the effectiveness of partial flow mode on the pressure drop penalty effect, and explain how and why the system performance is influenced by power capacities. Equations (29)–

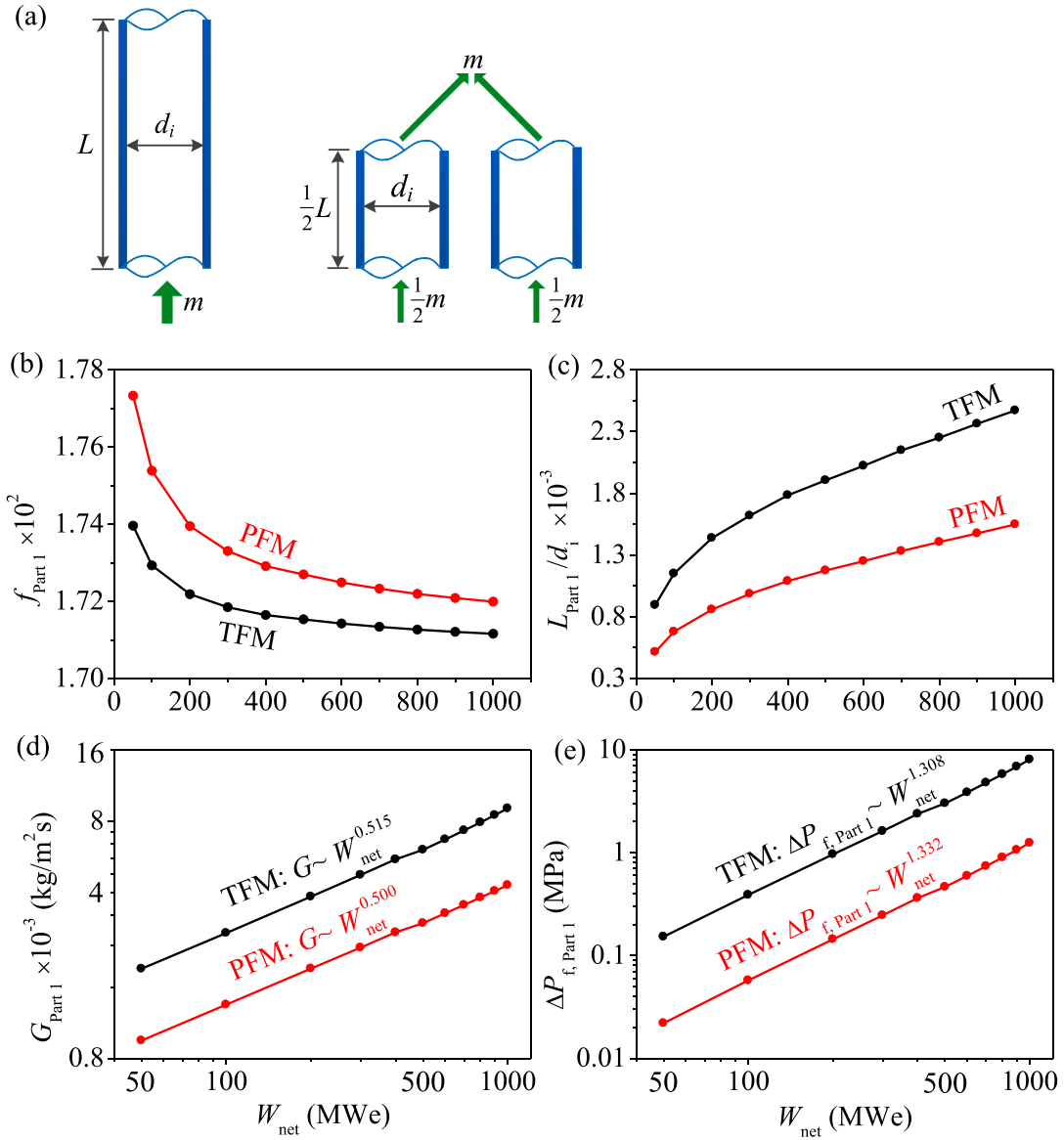


Fig. 7. Pressure drop reduction mechanism (a: ideal partial flow mode converted from total flow mode; b: frictional factors; c: length to diameter ratio; d: mass fluxes in Part 1; e: frictional pressure drops in Part 1).

(32) are called the scale laws, focusing on the furnace size L , mass flux G , surface to volume ratio A_b/V_b , length to volume ratio L/V_b and friction pressure drop ΔP_f dependent on power capacities, which are sufficient to attain the target of this paper. Because power plant is a complicated system and contains many engineering technical details, the scale laws for other parameters beyond Eqs. (29)–(32) are difficult to be achieved currently but will be tried in future.

Fig. 5a-b shows the calculated A_b/V_b and w_x/V_b using log-log plots, showing increased surface to volume ratio and length to volume ratio when decreasing power capacities. The curve fittings give

$$\begin{cases} \frac{A_b}{V_b} \sim W_{\text{net}}^{-0.510} \text{ for TFM and } \sim W_{\text{net}}^{-0.495} \text{ for PFM} \\ \frac{w_x}{V_b} \sim W_{\text{net}}^{-0.849} \text{ for TFM and } \sim W_{\text{net}}^{-0.827} \text{ for PFM} \end{cases} \quad (35)$$

The practical scale law in Eq. (35) supports the theoretically determined one in Eq. (31). At smaller W_{net} , larger A_b/V_b and L/V_b ensure easier arrangement of flow passages to reduce pressure drop, which is evidenced by larger number of tubes per unit power capacity in Fig. 5c. This scale law is similar to microchannel heat exchangers [32,33].

Microchannels have large surface to volume ratio to enhance heat transfer, while small power capacity provides larger surface area to volume ratio to reduce pressure drop. Fig. 5c shows the doubled number of tubes for PFM compared to TFM.

Fig. 6a-b shows furnace sizes $w_x = w_y$ and H_b , which are smaller when decreasing power capacities. The curves $w_x \sim W_{\text{net}}$ and $H_b \sim W_{\text{net}}$ also agree with the scale law given by Eq. (29). At larger W_{net} , furnace size shows difference between TFM and PFM. Later we will show that TFM has lower thermal efficiency than PFM. Thus, TFM needs larger furnace size to adapt larger coal consumption rate. Fig. 6c-d shows volume heat fluxes q_v and surface heat fluxes q_A , demonstrating increased q_v at smaller W_{net} , but insensitive q_A on W_{net} . A practical boiler approaches constant surface heat flux at different power capacities. Our calculated q_v and q_A are verified to be smaller than the limit range values for boiler design. For example, q_v at $W_{\text{net}} = 600$ MWe is smaller than the range value of 80–95 kW/m³ for steam-water boiler at similar condition. The volume heat flux in burning-out zone q_{bv} is important to verify if coal can be completely combusted (see Fig. 6e). The answer is yes, for example, q_{bv} at 1000 MWe is apparently lower than the ranged value of 200–260 kW/m³.

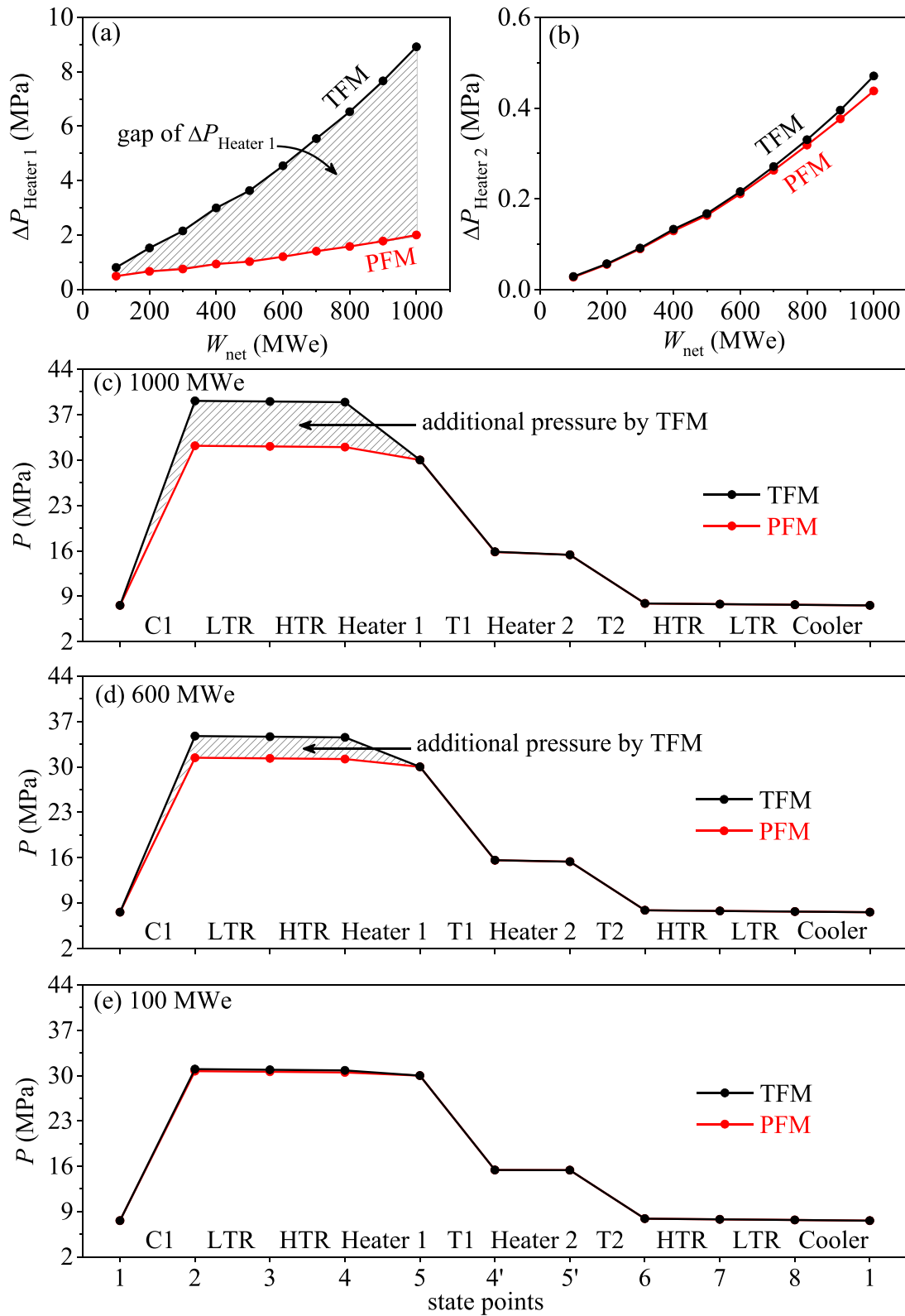


Fig. 8. Pressure distributions in cycle (a: pressure drops in Heater 1; b: pressure drops in Heater 2; c: $P_{2,\text{TFM}} = 39.12$ MPa and $P_{2,\text{PFM}} = 32.20$ MPa at 1000 MWe; d: $P_{2,\text{TFM}} = 34.75$ MPa and $P_{2,\text{PFM}} = 31.40$ MPa at 600 MWe; e: $P_{2,\text{TFM}} = 31.01$ MPa and $P_{2,\text{PFM}} = 30.69$ MPa at 100 MWe).

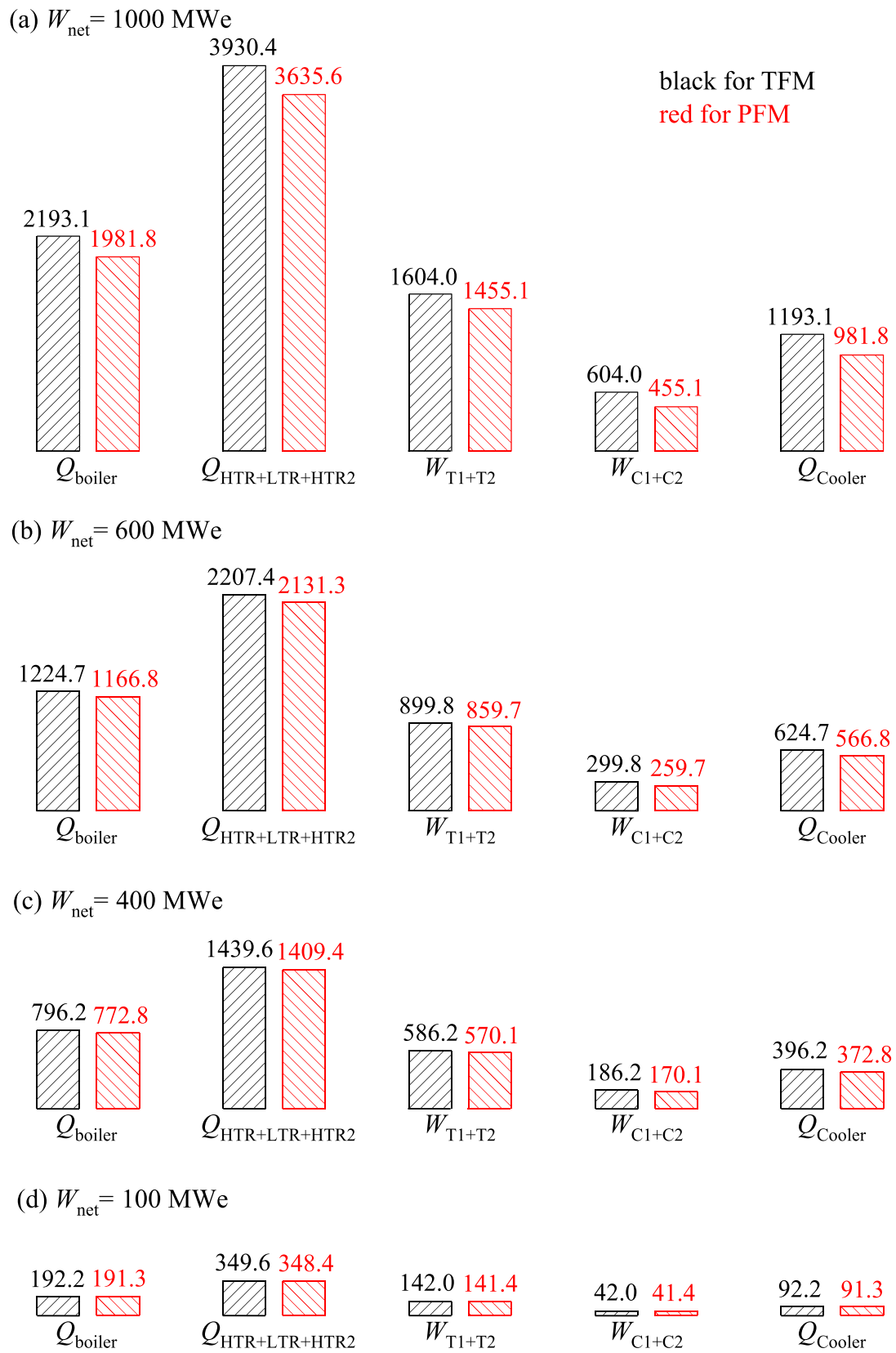


Fig. 9. Energy distribution in the cycle at power capacities of 1000, 600, 400 and 100 MWe (note: all the units are MW).

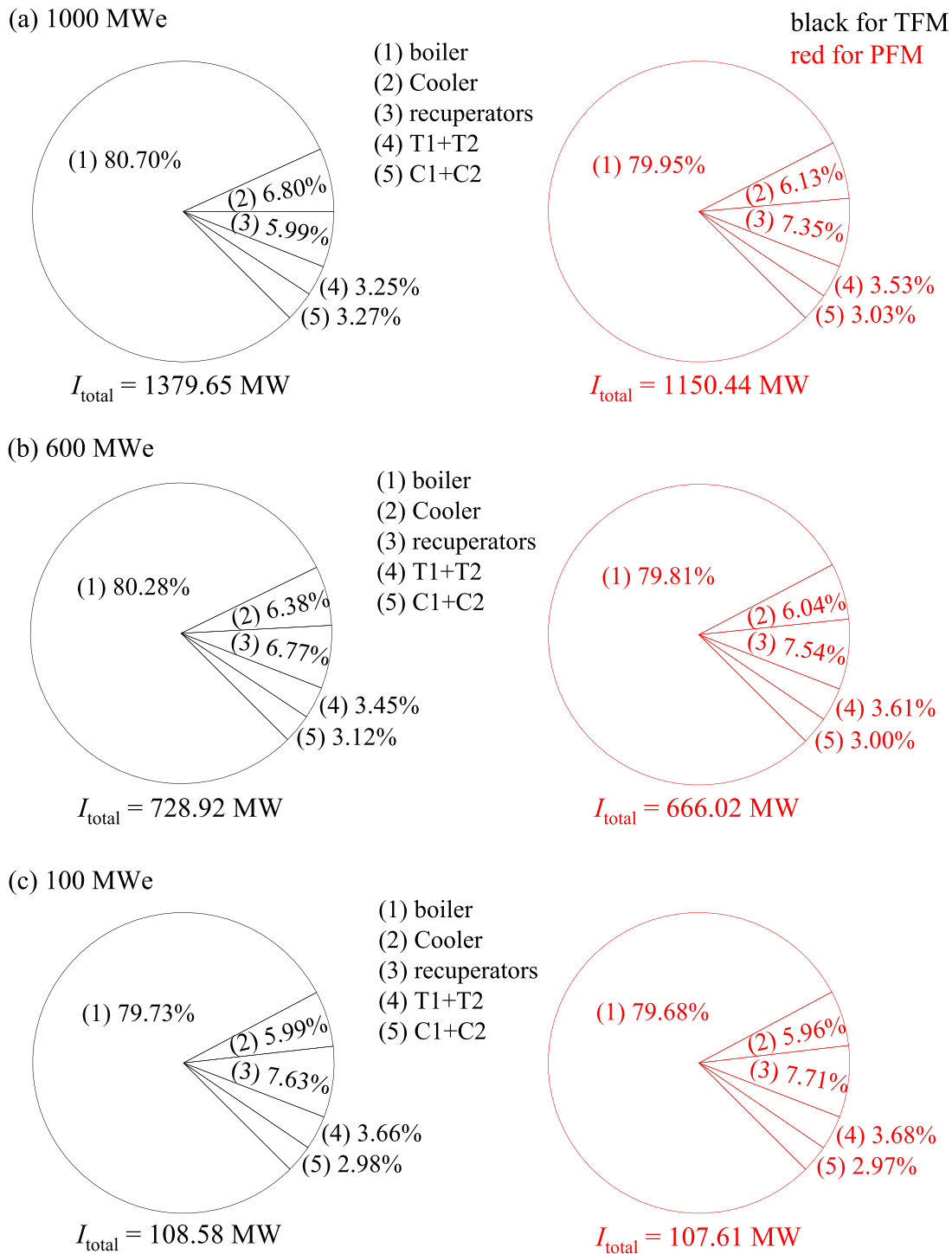


Fig. 10. Exergy destruction distributions in the cycle at power capacities of 1000, 600 and 100 MWe.

4.2. Pressure distribution in the system

Fig. 7a shows the ideal partial flow mode (PFM), in which two sections are parallelly connected, each having half tube length and half flow rate. How PFM reduces pressure drops is explored. Neglecting the variation of physical properties for CO₂, frictional pressure drop $\Delta P_f = f \cdot \frac{L}{d_i} \cdot \frac{G^2}{2\rho}$ is influenced by f , L/d_i and G . Because at high Re, f is more sensitive to wall roughness than mass flux (see Eq. (22)), f shows weak difference

between TFM and PFM (see Fig. 7b). We show significant decrease of $L_{Part 1}/d_i$ for PFM compared to TFM, where $L_{Part 1}$ is the Part 1 length in Fig. 7c. Due to the non-uniform heat load distribution along furnace height, $L_{Part 1}$ for PFM is not exactly the half of that for TFM. At same W_{net} , G for PFM is almost the half of that for TFM (see Fig. 7d). The practical scale law of $G \sim W_{net}^{0.5}$ agrees with the theoretically determined one by Eq. (30), where the exponent index is ~ 0.5 instead of $2/3$.

The data trends in Fig. 7b-d yield frictional pressure drops in Part 1

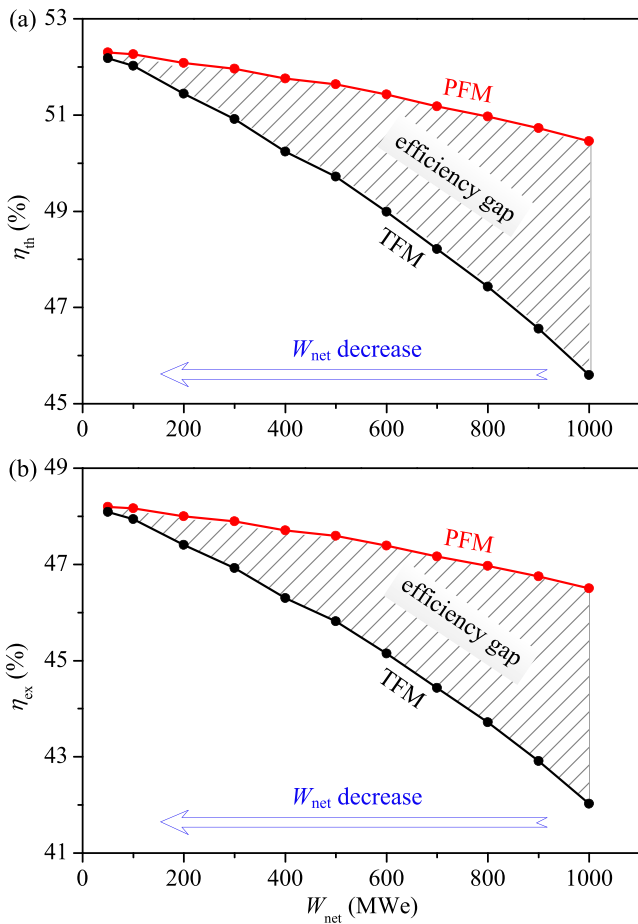


Fig. 11. Thermal efficiency and exergy efficiency at different power capacities.

shown in Fig. 7e. At larger W_{net} , huge difference exists between TFM and PFM. For the former, ΔP_f is 8.05 MPa at 1000 MWe, which is not acceptable for practical operation, but PFM reduces ΔP_f to 1.25 MPa. Hence, the conventional one-through water-steam boiler is not suitable for sCO_2 boiler, for which the partial flow strategy is necessary. With decrease of power capacities, the difference between TFM and PFM decreases. At small capacity such as 100 MWe, pressure drops for both the two modes are acceptable, under which sCO_2 operates well even without flow splitting. Fig. 7e supports the scale laws given in Eqs.32 and 34, in which the exponent index based on both theoretical prediction and practical calculation is ~ 1.3 in the scale law.

In summary, Fig. 7 can be explained by Eqs.32 and 34. Larger power capacities relatively narrowed flow passages for CO_2 flow to raise mass fluxes, accounting for increased pressure drops with increase of power capacities. Compared to TFM, PFM divides the total flow rate into two streams and uses short module length, explaining the significantly reduced pressure drop. The effect of physical properties of CO_2 on pressure drops is discussed. The identical vapor temperature at turbine inlet of 620 °C ensures very similar fluid temperature distributions at different power capacities for both TFM and PFM. The CO_2 temperatures have similar effect on pressure drops for all the conditions. Even though the CO_2 pressure at turbine inlet is kept as 30 MPa, pressures in heater tubes are different due to different pressure drops in various heater modules. The varied pressures in heater tubes in turn influence the physical properties of CO_2 to influence pressure drops, in which density ρ and viscosity μ should be concerned (see Eqs. (21) and (23)). An example is given here. At $T = 600$ °C, $\mu = 40.233 \times 10^{-6}$ Pa·s at 30 MPa shows small difference with $\mu = 41.876 \times 10^{-6}$ Pa·s at 40 MPa. However, $\rho = 170.89$ kg/m³ at 30 MPa is 22.9% smaller than $\rho = 221.68$ kg/m³ at 40 MPa. Once other parameters are identical, for PFM a lower

pressure 30 MPa in tubes yields an $\sim 30\%$ increase of pressure drop, compared to 40 MPa operation for TFM. In fact, pressure drop for PFM is only $\sim 1/8$ of that for TFM. Hence, the increase trend of pressure drop due to lower pressure operation is thoroughly suppressed by the decrease trend by using PFM. For all the conditions, laminar flow is never encountered, even at the smallest power capacity.

Fig. 8a-b illustrates pressure drops in Heaters 1 and 2. For TFM, Heater 1 includes Part 1 and SH1, but for PFM, Heater 1 involves one stream of Part 1 and SH1 parallelly connected with another stream of Part 2 and SH2, the two streams sharing same pressure drop. Part 1 and Part 2 belong to cooling wall modules, while other modules are suspended in flue channel. The curves of Fig. 8a are similar to those of Fig. 7e, indicating Part 1 or Part 2 dominates pressure drops. Fig. 8b shows that pressure drops in Heater 2 are almost one-magnitude smaller than Heater 1.

Fig. 8c-e examines the distribution of pressures along the cycle. Pressure difference across inlet and outlet of a component is the value that is supplied or consumed by such a component. Compressors 1 and 2 elevate pressures, but other components consume pressures. An ideal condition is that the pressures supplied by compressors are thoroughly consumed by turbines. Practical operation deviates from the ideal condition, due to pressure drops in various heat exchangers. The pressure at C1 outlet reaches maximum along a cycle. At 1000 MWe using TFM, C1 provides an additional 9.12 MPa beyond 30 MPa at T1 inlet. This additional pressure is majorly consumed by Heater 1, regarded as a CO_2 blockage phenomenon, just like blood capillary blockage for mankind. Evidenced by a 2.20 MPa additional pressure supplied by C1, PFM alleviates the CO_2 blockage phenomenon. Smaller power capacity gradually weakens the CO_2 blockage phenomenon. At the capacity of 100 MWe, the additional pressure that needs to be supplied by C1 is only 1.01 MPa for TFM and 0.69 MPa for PFM.

4.3. Energy, exergy and efficiency of the system

A sCO_2 power plant receives energy Q_{boiler} due to coal combustion, dissipates extra heat Q_{cooler} to environment, produces mechanical power W_{T1+T2} , and consumes mechanical power W_{C1+C2} for compression. Regenerative heat exchangers recycle heat in the system, which is not involved for energy balance analysis. The energy conservation equation is

$$Q_{boiler} + W_{C1+C2} = W_{T1+T2} + Q_{cooler} \quad (36)$$

Where the left side and right side of Eq. (36) represent energy input and output, respectively. Rewriting Eq. (36) as

$$W_{net} = W_{T1+T2} - W_{C1+C2} = Q_{boiler} - Q_{cooler} \quad (37)$$

Remembering W_{net} as the power capacity, we plot energy distribution in the system, see comparative columns in Fig. 9. At given W_{net} using TFM, turbines shall produce more power than PFM, other energy terms are also elevated consecutively, explaining higher black columns than red columns. The pressure drop penalty effect is significant for large scale power generation. Compared to PFM, TFM increases compression power by 32.7% and 15.4% at 1000 MWe and 600 MWe respectively, but the difference is only 1.4% at 100 MWe. In summary, TFM generates additional load to compressors, hence more power shall be consumed, PFM greatly reduces additional power consumption. The difference between TFM and PFM decreases when decreasing power capacities.

Exergy destruction in the system is shown in Fig. 10. Due to large irreversibility in combustion process and large temperature difference between combustion flame and CO_2 in tubes, the exergy destruction in boiler accounts for $\sim 80\%$ of the total exergy destruction (I_{total}), agreeing with Ref. [34]. All the other components except boiler account for $\sim 20\%$ of I_{total} . TFM elevates the exergy destruction level over the whole system compared to PFM. At 1000 MWe, TFM increases I_{total} by 19.9% than PFM, this increment becomes 9.4% at 600 MWe. Only 0.9%

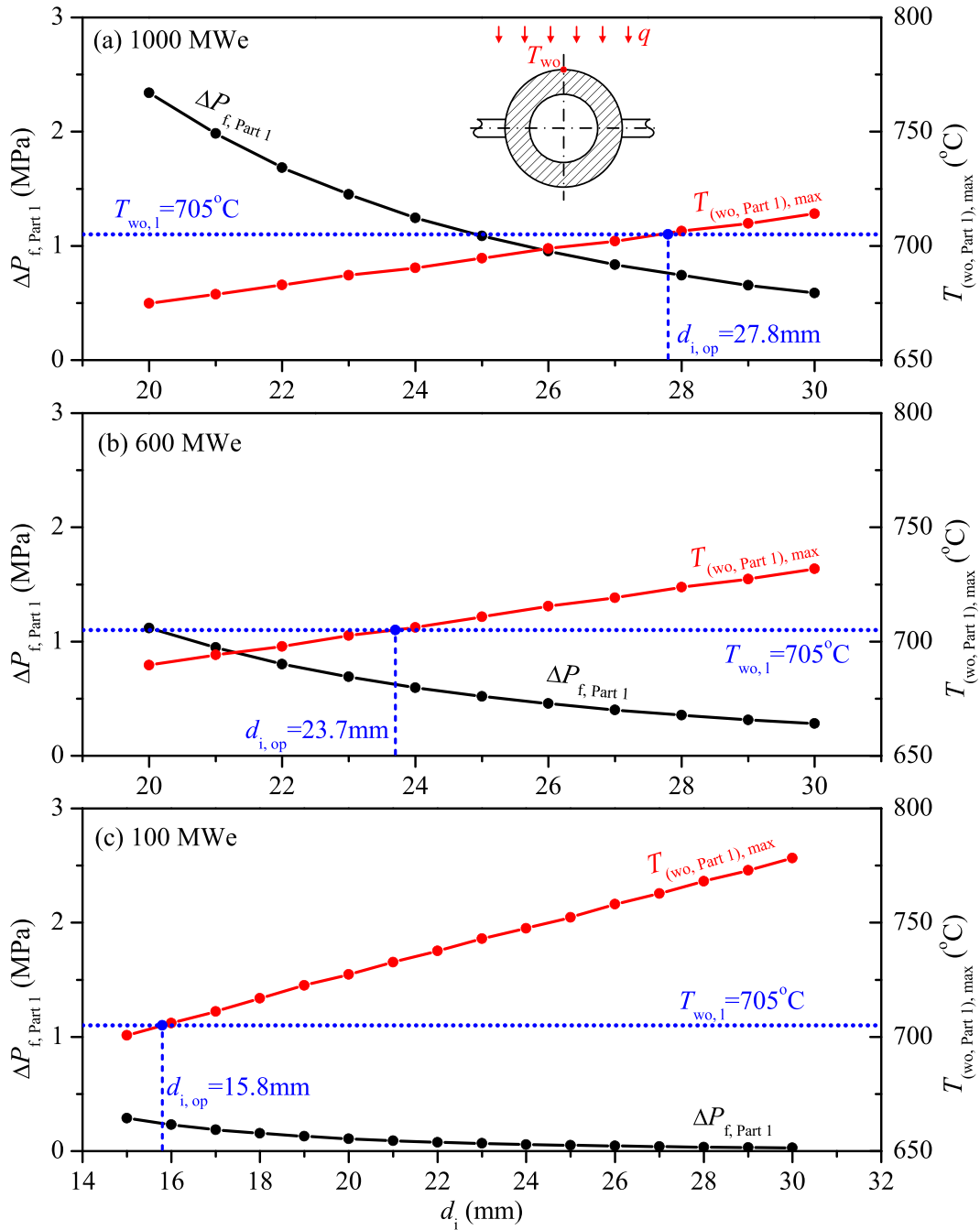


Fig. 12. Pressure drops and wall temperatures dependent on inner tube diameters to search optimum values.

difference of I_{total} exists at 100 MWe between TFM and PFM. We note that entropy generation S_g is proportional to exergy destruction i as $i = T_0 S_g$, where T_0 is the referenced environment temperature [35]. Hence, Fig. 10 also indicates that boiler has the largest contribution to the entropy generation due to combustion process.

Thermal efficiency and exergy efficiency of the whole system are presented in Fig. 11. Both η_{th} and η_{ex} decrease with increase of W_{net} , but the slopes of curves are quite different for TFM and PFM. The former displays steeper gradient than the latter, showing more sensitivity of efficiencies versus power capacities for TFM. Efficiencies of PFM are always larger than TFM, generating efficiency gaps to form triangle distributions enclosing $\eta_{th} \sim W_{net}$ and $\eta_{ex} \sim W_{net}$ curves. The efficiency gap is large at large W_{net} but shortened at small W_{net} . At 1000 MWe, PFM

has $\eta_{th} = 50.46\%$, but the value becomes 45.60% for TFM. At 100 MWe, almost identical efficiencies exist to have $\eta_{th} = 52.27\%$ for PFM and 52.02% for TFM. Exergy efficiency shows similar behavior with thermal efficiency. We conclude significant pressure drop penalty effect and sensitive variation of efficiencies versus power capacities for TFM. The pressure drop effect is greatly weakened with PFM.

The scale laws of furnace sizes, mass fluxes and frictional pressure drops versus power capacities are proposed, agreeing with numerical simulations. They explain how and why the system performance is influenced by power capacities. At small W_{net} such as 100 MWe, the surface area to volume ratio is larger to provide sufficient flow passage, thus the pressure drop penalty effect is weak. With increase of W_{net} , the pressure drop penalty effect increases, raising compressor load to

provide additional pressure beyond the pressure to drive turbines. The pressure drop penalty effect elevates the levels of energy loads and exergy destructions in the system. Because partial flow mode (PFM) reduces pressure drops to $\sim 1/8$ of those for total flow mode (TFM), it eliminates the pressure drop penalty effect. Hence, one can enjoy higher sCO₂ cycle efficiency than the widely used water-steam Rankine cycle.

The performance of a power plant is influenced by many factors, including vapor temperature and pressure at turbine inlet, turbine and compressor efficiencies and pressure drops in components. Here, we assume constant isentropic efficiencies of turbine and compressors. Main vapor parameters are 30 MPa/620 °C at turbine inlet. Thus, the pressure drop penalty effect can be decoupled from comprehensive effects. sCO₂ cycle is in developing stage, many works are to be done [36]. Currently, experimental data are achieved for small systems (10 kW–1 MWe) [36]. Issues such as CO₂ leakage have been encountered, but may be weakened for large systems (>10 MWe) [37]. Small turbomachines use radial-type, but large scale uses axial-type (>30 MWe for turbines and >100 MWe for compressor), hence efficiencies are weakly influenced by capacities [37,38]. One may mention the better performance for large systems, which seems to be true for water-steam Rankine cycle that has been evolved for one century. In this history, small capacity corresponds to low vapor parameters. In the early stage, the 100 MWe power plant had vapor parameters of 8.8 MPa/535 °C, but now vapor parameters reach 30 MPa and ~ 700 °C [39]. Besides, small power plant did not use reheating, but large-scale utilization uses reheating. In summary, lower efficiency of steam-water Rankine cycle is caused by lower vapor parameters and bad cycle design, not caused by small capacity.

The connection among pressure drop, thermal efficiency and power capacity is summarized here. Usually, mass flow rate of sCO₂ cycle is several times of that for water-steam Rankine cycle, causing ultra-large pressure drop to severely deteriorate system performance. Along the increase roadmap of power capacities, flow passages are not sufficient to raise mass flux, increasing pressure drops of boiler. Thus, thermal efficiency decreases to conclude serious pressure drop penalty effect with increase of power capacities. Alternatively, with decrease of power capacities, the pressure drop penalty effect is weakened to yield improved system performance (see Fig. 11). The partial flow mode significantly weakens the pressure drop penalty effect, until there is no difference between TFM and PFM at very small power capacity such as $W_{\text{net}} < 100$ MWe. As mentioned above, the thermal efficiency of system is influenced by various factors. Our present study decoupled the pressure drop penalty effect from comprehensive effects by keeping identical vapor pressures and temperatures for all the cases. The combined effects of pressure drop and main vapor parameters at different power capacities will be investigated in the future.

Here, we use $d_i = 24$ mm for all the cases, where d_i is the inner diameter of cooling wall tubes. Such size approaches but is not the exactly optimum value. Extra studies were performed using d_i as a variable. Three power capacities of 1000 MWe, 600 MWe and 100 MWe were calculated (see Fig. 12). Pressure drops decrease with increase of d_i . Alternatively, larger d_i suppresses heat transfer coefficients of CO₂ in tubes and increases tube wall thickness. The outcome is the increased outer wall temperatures T_{wo} with increase of d_i . The optimum $d_{i,\text{op}}$ is located at the crossing point of wall temperature curve and temperature limit $T_{\text{wo},l}$. The material of Super 304H corresponds to $T_{\text{wo},l} = 705$ °C. The three power capacities of $W_{\text{net}} = 1000$ MWe, 600 MWe and 100 MWe yield the optimal $d_i = 27.8$ mm, 23.7 mm and 15.8 mm, respectively, at which thermal efficiencies are 50.83%, 51.40% and 52.16%, approaching 50.46%, 51.42% and 52.27% at the fixed $d_i = 24.0$ mm. We note that these results are obtained for partial flow mode.

In this paper the steady and designed conditions are treated. Under non-uniform heating, the partial flow mode can be fulfilled by two different ways. One is to set the half flow rate in each of the two heater modules with different module lengths, just like that used in this paper. Alternatively, the two module lengths are the same with different flow

rates in the two modules. The two methods correspond to different control strategies. The former needs to control the same flow rate in the two modules, but the latter needs to control the exit vapor temperatures of the two modules to be identical.

The transient analysis is important for the safe and economic operation of a power plant [40]. The partial flow mode induces the modular boiler design to form a flow network. The effect of partial flow mode on the system dynamics is analyzed here. The residence time of CO₂ in tubes (τ) affects system dynamics, noting that τ is scaled as $\tau \sim L/u = \rho L/G$, where u is the axial flow velocity in tubes. Compared to total flow mode, partial flow mode reduces module length and mass flux to be half simultaneously. Hence, the flow segment weakly changes the residence time. From this aspect, the partial flow mode may not change the response time with respect to the load variations. Attention should be paid on the control of the exit vapor temperatures for different heater modules. The transient operation or load variation causes the exit vapor temperature of each module to deviate from the rated value. Numerical simulations regarding the transient analysis are expected in the future.

5. Conclusions

Following conclusions are drawn based on current studies:

1. A numerical model was proposed to analyze sCO₂ coal fired power plants at various power capacities. The sCO₂ cycle uses the overlap energy utilization strategy, eliminating efficiency difference between top and bottom cycles. The boiler designs with total flow mode and partial flow mode are illustrated to incorporate heater modules with cycle.
2. The proposed scale laws include characteristic boiler size, size to volume ratio, surface to volume ratio, mass flux and frictional pressure drop dependent on power capacities, explaining how and why system performance is influenced by power capacities.
3. With increase of W_{net} , the narrowed flow passages of CO₂ increase pressure drops, hence compressors shall supply additional pressure and load beyond to drive turbines. This effect increases energy loads and exergy destructions in the system to deteriorate its performance.
4. PFM significantly decreases pressure drops, lowering the extra pressures and loads of compressors beyond to drive turbines to acceptable levels. PFM has much higher efficiencies than TFM, which are more obvious along the increase roadmap of W_{net} .
5. We conclude the necessary application of PFM for large scale power generation. PFM may not be used only at small $W_{\text{net}} < 100$ MWe, under which the surface to volume ratio is sufficient to arrange more flow passages of CO₂ in boiler tubes.

Declaration of Competing Interest

The authors declare that they have no known competing financial interests or personal relationships that could have appeared to influence the work reported in this paper.

Acknowledgements

This work was supported by the National Key R&D Program of China (2017YFB0601801), and the Natural Science Foundation of China (51821004).

Appendix

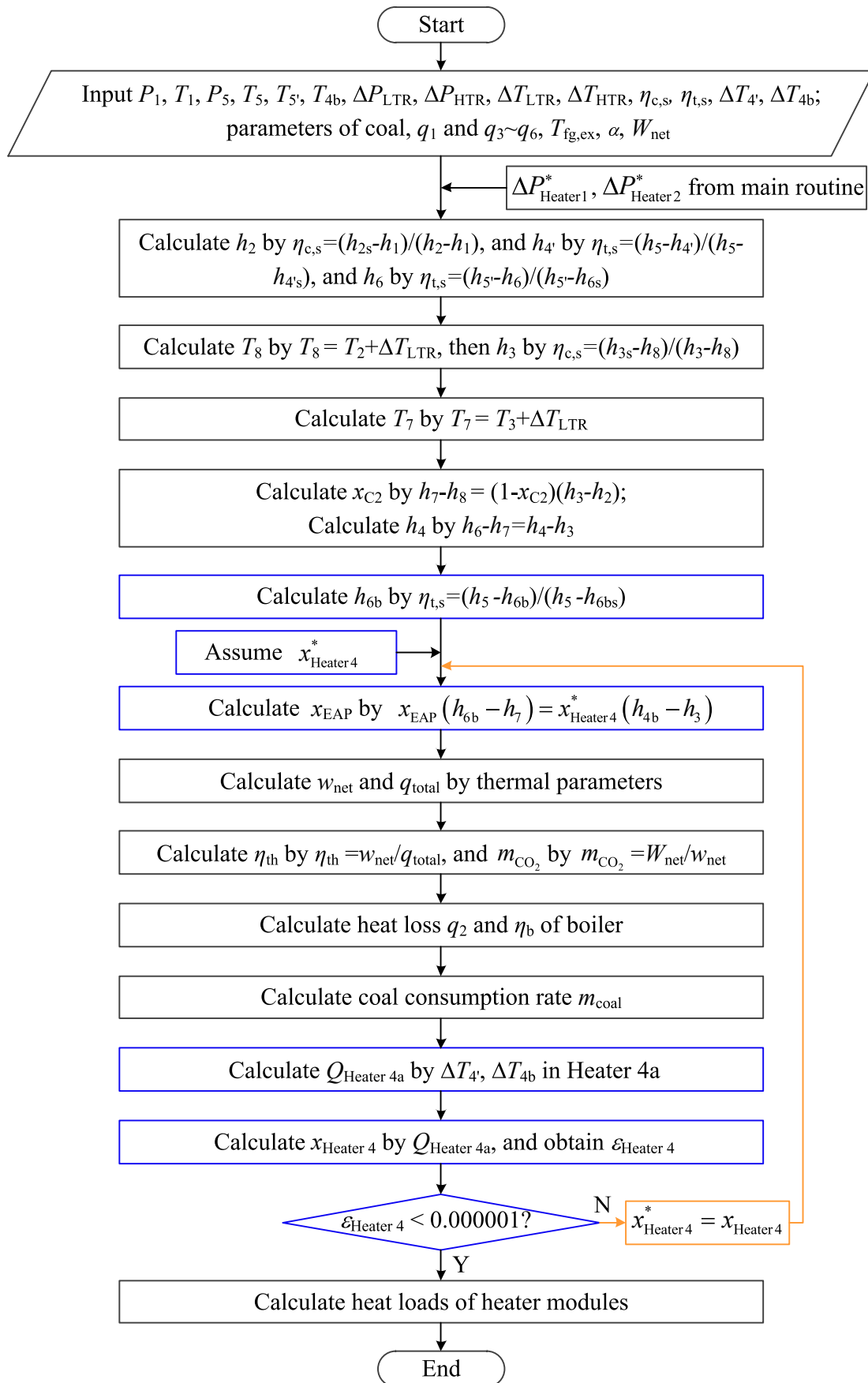


Fig. A1. Computation scheme of thermodynamic cycle.

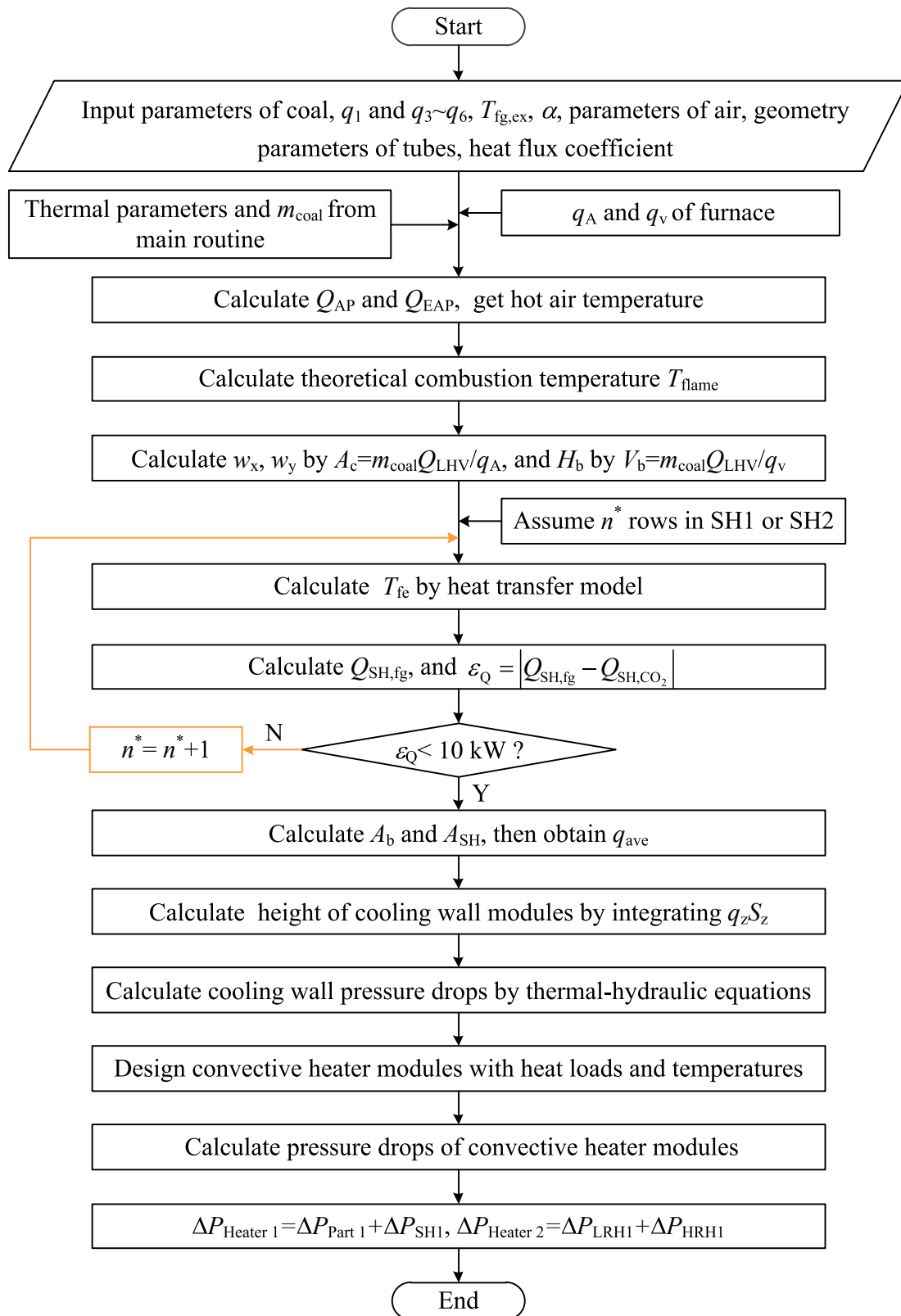


Fig. A2. Computation scheme of boiler design and thermal-hydraulic characteristics.

References

- [1] Dostal V, Hejzlar P, Driscoll MJ. The supercritical carbon dioxide power cycle: comparison to other advanced power cycles. Nucl Technol 2006;154(3):283–301.
- [2] Li MJ, Zhu HH, Guo JQ, Wang K, Tao WQ. The development technology and applications of supercritical CO₂ power cycle in nuclear energy, solar energy and other energy industries. Appl Therm Eng 2017;126:255–75.
- [3] Ahn Y, Bae SJ, Kim M, Cho SK, Baik S, Lee JI, et al. Review of supercritical CO₂ power cycle technology and current status of research and development. Nucl Eng Technol 2015;47:647–61.

- [4] Feher EG. The supercritical thermodynamic power cycle. *Energy Convers Manage* 1968;8:85–90.
- [5] Dostal V. A supercritical carbon dioxide cycle for next-generation nuclear reactors. Department of Nuclear Engineering. USA: Massachusetts Institute of Technology; 2004.
- [6] Wang K, He YL. Thermodynamic analysis and optimization of a molten salt solar power tower integrated with a recompression supercritical CO₂ Brayton cycle based on integrated modeling. *Energy Convers Manage* 2017;135:336–50.
- [7] Pérez-Pichel GD, Linares JI, Herranz LE, Moratilla BY. Thermal analysis of supercritical CO₂ power cycles: Assessment of their suitability to the forthcoming sodium fast reactors. *Nucl Eng Des* 2012;250:23–34.
- [8] Novales D, Erkoreka A, De la Peña V, Herrazti B. Sensitivity analysis of supercritical CO₂ power cycle energy and exergy efficiencies regarding cycle component efficiencies for concentrating solar power. *Energy Convers Manage* 2019;182:430–50.
- [9] Xu J, Sun E, Li M, Liu H, Zhu B. Key issues and solution strategies for supercritical carbon dioxide coal fired power plant. *Energy* 2018;157:227–46.
- [10] Sun E, Xu J, Li M, Liu G, Zhu B. Connected-top-bottom-cycle to cascade utilize flue gas heat for supercritical carbon dioxide coal fired power plant. *Energy Convers Manage* 2018;172:138–54.
- [11] Sun E, Xu J, Hu H, Li M, Miao Z, Yang Y, et al. Overlap energy utilization reaches maximum efficiency for S-CO₂ coal fired power plant: A new principle. *Energy Convers Manage* 2019;195:99–113.
- [12] Gu M, Wang M, Chen X, Wang J, Lin Y, Chu H. Numerical study on the effect of separated over-fire air ratio on combustion characteristics and NO_x emission in a 1000 MW supercritical CO₂ boiler. *Energy* 2019;175:593–603.
- [13] Brun K, Friedman P, Dennis R. Fundamentals and applications of supercritical carbon dioxide (sCO₂) based power cycles. Oxford: Woodhead Publishing; 2017.
- [14] Le Moulec Y. Conceptual study of a high efficiency coal-fired power plant with CO₂ capture using a supercritical CO₂ Brayton cycle. *Energy* 2013;49:32–46.
- [15] Yang Y, Bai W, Wang Y, Zhang Y, Li H, Yao M, et al. Coupled simulation of the combustion and fluid heating of a 300 MW supercritical CO₂ boiler. *Appl Therm Eng* 2017;113:259–67.
- [16] Zhou J, Xiang J, Su S, Hu S, Wang Y, Xu K, et al. Key issues and practical design for cooling wall of supercritical carbon dioxide coal-fired boiler. *Energy* 2019;186: 115834.
- [17] Cabeza LF, de Gracia A, Fernández AI, Farid MM. Supercritical CO₂ as heat transfer fluid: a review. *Appl Therm Eng* 2017;125:799–810.
- [18] Ehsan MM, Guan Z, Klimenko AY. A comprehensive review on heat transfer and pressure drop characteristics and correlations with supercritical CO₂ under heating and cooling applications. *Renew Sust Energy Rev* 2018;92:658–75.
- [19] Chang S, Zhuo J, Meng S, Qin S, Yao Q. Clean coal technologies in China: Current status and future perspectives. *Engineering* 2016;2:447–59.
- [20] Ackermann T, Andersson G, Soder L. Distributed generation: a definition. *Electr Pow Syst Res* 2001;57:195–204.
- [21] Che D. Boilers-Theory Design and Operation. Xi'an: Xi'an Jiaotong University Press; 2008.
- [22] Padilla RV, Soo Too YC, Benito R, Stein W. Exergetic analysis of supercritical CO₂ Brayton cycles integrated with solar central receivers. *Appl Energy* 2015;148: 348–65.
- [23] Turchi CS, Ma Z, Neises TW, Wagner MJ. Thermodynamic study of advanced supercritical carbon dioxide power cycles for concentrating solar power systems. *J Sol Energy Eng* 2013;135:041007.
- [24] Li QD, Liu ZZ. Thermal economy calculation and analysis of thermal power plant. Beijing: China Electric Power Press; 2008 [in Chinese].
- [25] Sarkar J. Second law analysis of supercritical CO₂ recompression Brayton cycle. *Energy* 2009;34:1172–8.
- [26] Fu QS. Thermodynamic analysis method of energy system. Xi'an: Xi'an Jiaotong University Press; 2005 [in Chinese].
- [27] Guide on selection of furnace characteristic parameters for large pulverized coal fired boilers. Power industry standards of P.R.C, DL/T 831-2015 [in Chinese].
- [28] Wang C. The change in boiler's capacities affects the furnace combustion and selecting technique for furnace's construction parameters. *Boiler Technology* 2008; 03:17–20 [in Chinese].
- [29] Chen D, Fan C, Yang Y, Zhang F, Zhu C. Study on water wall temperature and heat load distribution in 1000MW tower-type once-through boilers. *J Chinese Soci Power Eng* 2013;33(5):229–334 [in Chinese].
- [30] Wang Z, Sun B, Wang J, Hou L. Experimental study on the friction coefficient of supercritical carbon dioxide in pipes. *Int J GreenH Gas Con* 2014;25:151–61.
- [31] Seamless stainless steel tubes for boiler and heat exchanger. National standards of P.R.C, GB 13296-2013 [in Chinese].
- [32] Luo L, Fan Y, Daniel T. Heat exchanger: from micro- to multi-scale design optimization. *Int J Energ Res* 2007;31:1266–74.
- [33] Khan MG, Fartaj A. A review on microchannel heat exchangers and potential applications. *Int J Energ Res* 2011;35:553–82.
- [34] Si N, Zhao Z, Su S, Han P, Sun Z, Xu J, et al. Exergy analysis of a 1000 MW double reheat ultra-supercritical power plant. *Energy Convers Manage* 2017;147:155–65.
- [35] Som SK, Datta A. Thermodynamic irreversibilities and exergy balance in combustion processes. *Prog Energy Combust Sci* 2008;34:351–76.
- [36] Xu J, Liu C, Sun E, Xie J, Li M, Yang Y, et al. Perspective of S-CO₂ power cycles. *Energy* 2019;186:115831.
- [37] Fleming D, Holschuh T, Conboy T, Rochau G, Fuller R. Scaling considerations for a multi-megawatt class supercritical CO₂ Brayton cycle and path forward for commercialization. In: ASME, editor. Proceedings of ASME Turbo Expo 2012: Turbine Technical Conference and Exposition, Copenhagen, Denmark; June 11-15, 2012.
- [38] Cho SK, Bae SJ, Jeong Y, Lee J, Lee JI. Direction for high-performance supercritical CO₂ centrifugal compressor design for dry cooled supercritical CO₂ Brayton cycle. *Appl Sci* 2019;9(4057):1–20.
- [39] Abe F. Research and development of heat-resistant materials for advanced USC power plants with steam temperatures of 700 °C and above. *Engineering* 2015;1 (2):211–24.
- [40] Wu X, Shen J, Wang M, Lee KY. Intelligent predictive control of large-scale solvent-based CO₂ capture plant using artificial neural network and particle swarm optimization. *Energy* 2020;196:117070.